https://doi.org/10.5194/egusphere-2024-3761
Preprint. Discussion started: 30 January 2025

Tropical Ozone Trends (1998 to 2023): A Synthesis from SHADOZ, IAGOS and OMI/MLS Observations

Anne M. Thompson[1,2*], Ryan M. Stauffer[1], Debra E. Kollonige[1,3], Jerald R. Ziemke[1,4], María Cazorla[5], Pawel Wolff[6], Bastien Sauvage[7]

[1]NASA/Goddard Space Flight Center (GSFC), Greenbelt, MD, USA anne.m.thompson@nasa.gov; ORCID: 0000-0002-7829-0920; ryan.m.stauffer@nasa.gov; ORCID: 0000-0002-8583-7795; [2]University of Maryland-Baltimore County, Baltimore, MD 21228; [3]Science Systems and Applications, Inc., Lanham, MD, debra.e.kollonige@nasa.gov; ORCID: 0000-0002-6597-328X; [4]Morgan State Univ., Baltimore, MD, jerald.r.ziemke@nasa.gov; ORCID: 0000-0002-5575-3654; ; [5]Universidad San Francisco de Quito USFQ, Colegio de Ciencias e Ingenierías, Instituto de Investigaciones Atmosféricas, Quito, Ecuador; mcazorla@usfq.edu.ec; https://orcid.org/0000-0001-5295-2968

[6] SEDOO, Univ. Paul Sabatier III, Toulouse, France; pawel.wolff@aero.obs-mip.fr; ORCID: 0000-0002-2082-6825; [7] Laboratoire d'Aérologie Observatoire Midi-Pyrénées, 14 av. E. Belin, 31400 Toulouse France; Bastien.sauvage@univ-tlse3.fr; ORCID : 0000-0003-3410-2139

*Corresponding author: Anne M. Thompson (anne.m.thompson@nasa.gov)

Keywords: **Ozonesondes, Ozone Trends, Lower Stratosphere, Satellite Ozone, SHADOZ, IAGOS**

https://doi.org/10.5194/egusphere-2024-3761
Preprint. Discussion started: 30 January 2025

Abstract. Trends in tropical tropospheric ozone over the past ~20-30 years have been reported using ozonesonde profiles from five SHADOZ sites (Thompson et al., 2021, "T21"; Stauffer et al., 2024, "S24") and a combination of satellite, SHADOZ and IAGOS aircraft measurements (Gaudel et al., 2024). Selected tropical sonde and aircraft trends are compared with other ground-based instruments in Van Malderen et al. (2024a). We have extended T21 for monthly-averaged five-station SHADOZ data with a Multiple Linear Regression (MLR) model, covering 1998 to 2023. We report: (1) trends in two free tropospheric (FT) ozone layers, lowermost stratosphere (LMS) ozone, total tropospheric column ($TrCO_{sonde}$) and tropopause height; (2) trends for 2000-2023 (no 1997-1998 ENSO) and 1998-2019 (no COVID-19). (3) $TrCO_{sonde}$ trends, 2005-2023, compared to OMI/MLS $TrCO_{satellite}$. The findings: (1) Extending SHADOZ trends four years does not change the T21 results: annual trends negligible except in one FT layer (Natal-Ascension) and for tropopause-referenced LMS. A slight reduction in FT trends may reflect a moderating effect of COVID-19. (2) Adding thousands of IAGOS profiles to the 5-site SHADOZ data similarly showed near-zero MLR trends ($p<0.05$) in a pressure-defined FT ozone layer (300-700 hPa); SHADOZ sampling is sufficient. (3) With the $TrCO_{sonde}$ adding 0-5 km ozone, trends are only detected over SE Asia and Natal-Ascension at 2-3%/decade, $p<0.05$; comparison to preliminary trends from the TOAR II/HEGIFTOM activity (a 0-300 hPa TrOC) gives similar results. For 2005-2023 MLR annually averaged trends for $TrCO_{sonde}$ and OMI/MLS $TrCO_{satellite}$ agree within uncertainties at 4 of 5 SHADOZ sites.

1 Introduction

The importance of tropical tropospheric ozone in atmospheric composition and climate variability has long been known. Although the thickness of total column ozone (TrCO) in the tropics (~250-325 Dobson Units, DU; 1 DU=2.69x10^{16}cm^{-2}) is much less than in the extra-tropics (350-450 DU), the latitude band from -30^{o} to +30^{o} covers roughly 1/3 of the Earth's surface. In this region tropospheric ozone is a major source of global OH (hydroxyl radical), key to Earth's oxidizing capacity (Thompson et al., 1992), controlling the lifetimes of countless biogenic and anthropogenic species. Global OH also controls the lifetime of methane, a powerful greenhouse gas with both natural and anthropogenic sources. Methane (CH_4) increases alone add ozone to the troposphere and methane's oxidation by OH to carbon monoxide (CO), that also affects the amount of OH, establishes a feedback cycle among O_3-OH-CH_4-CO. Regional variability in factors controlling the cycle derives from local levels of the shorter-lived nitrogen oxides and reactive VOC (volatile organic compounds). The same latitude band (-30^{o} to +30^{o}) is where the "tropical pipe" introduces ozone and other ozone-destroying or creating trace species into the lowermost stratosphere (LMS).

https://doi.org/10.5194/egusphere-2024-3761
Preprint. Discussion started: 30 January 2025

Thus, trends in tropical tropospheric and LMS ozone are of interest for several reasons. First, free tropospheric (FT) ozone is an important greenhouse gas. There is a potential for significant changes in FT ozone because parts of the tropics are in areas of rapid changes in emissions. These may be caused by economic development (Zhang et al., 2016) and/or variations in land-use and fire activity (Tsivlidou et al., 2023). Second, with relatively low ozone amounts relative to the extra-tropics, ozone in the tropical troposphere is more sensitive to dynamical interactions. The influences of climate oscillations on FT and LMS ozone have been documented with ozonesonde and satellite data (Thompson et al., 2001; Ziemke et al., 2003; Ziemke et al., 2006; Ziemke et al., 2019; Lee et al., 2010; Randel and Thompson, 2011; Thompson et al., 2011).

Context for this study comes from the International Global Atmospheric Chemistry/Tropospheric Ozone Assessment Report (IGAC/TOAR) that is completing its second phase, TOAR II, initiated in 2020. The first TOAR (Refer to *Elementa* collection of papers, 2014-2019) findings included an assessment of surface ozone changes based on a vast set of global surface ozone measurements. Ground-based observations for the FT were much more sparse, with uneven geographic coverage of ozone soundings (~60 publicly available records since the early 1990s) and aircraft landing and takeoff ozone profiles for the same period, only to ~300 hPa (Thouret et al., 2022). Efforts to fill gaps with tropospheric ozone estimates from satellite data were mixed. For the first TOAR Gaudel et al. (2018) pointed out that five satellite products covering the tropics and mid-latitudes for the 2005-2016 period differed from one another not only in magnitude but in sign as well. A recent evaluation of six updated satellite products, for 2004-2019 over the tropics only (Gaudel et al., 2024), where satellite estimates tend to be most reliable (Thompson et al., 2021), also exhibited a range of values. Accordingly, TOAR II decided to focus efforts for assessing FT on data from 5 global networks of ground-based (GB) instrumentation. The rationale is that GB networks, with stable operations at fixed sites with well-calibrated instruments (De Mazière et al., 2018) provide suitable time-series at dozens of sites.

During the TOAR study period we analyzed ozone profiles in the tropics collected in the Southern Hemisphere Additional Ozonesondes (SHADOZ) network (Thompson et al., 2003) to compute FT and LMS ozone trends. In Thompson et al. (2021, hereafter referred to as T21) we used data from 8 SHADOZ stations within $\pm$15 degrees latitude with the Goddard Multiple-Linear Regression (MLR) model to calculated trends from 1998 through 2019. Changes in layers between 5 and 15 km were relatively small, ~(1-3)%/decade at most, except over the equatorial SE Asian stations at Kuala Lumpur and Watukosek, Indonesia (**Table 1).**

More recently, in Stauffer et al. (2024, referred to as S24) we demonstrated that over the 25-yr period 1998-2022, early year (February through April/May) FT ozone increases are associated with declining convection, most pronounced over these same SE Asian locations but observed at other SHADOZ locations. With the newest OMI/MLS-based satellite estimates of total tropospheric column ozone

https://doi.org/10.5194/egusphere-2024-3761
Preprint. Discussion started: 30 January 2025

(TrCO), Gaudel et al. (2024) showed that during the Aura era (2005-2019) the satellite, SHADOZ and IAGOS aircraft profiles were in good agreement over SE Asia, similar to S24, but more divergent over the equatorial Americas and Africa. We also contributed analyses of SHADOZ and IAGOS to a global evaluation of tropospheric ozone (Van Malderen et al., 2024a; Van Malderen et al., 2024b) that included trends from lidar, FTIR and umkehr measurements from Dobson spectrometers. All the data in the latter studies were rigorously reprocessed in the TOAR II/Harmonization and Evaluation of Ground-based Instruments for Free-Tropospheric Ozone Measurements (HEGIFTOM) project that began in 2021. The HEGIFTOM-based trends used data from only selected SHADOZ stations and was restricted to below 300 hPa and the period 2000-2022. Here we revisit the SHADOZ record in the equatorial zone (-15^{o} to +15^{o}) using data from 1998 through 2023 to address the following questions:

- Compared to T21 what do FT and LMS ozone trends look like with four additional years of SHADOZ sonde data?
- Are there discernible impacts of COVID-19? How do trends in tropospheric ozone for 1998-2023 compare to trends for 2000 to 2023? Does the 26 year record show a sensitivity in changes due to SHADOZ starting at the end of the intense 1997-1998 ENSO?
- Do the 1998-2023 SHADOZ trends in the lower FT (defined as 700-300 hPa) change when augmented by thousands of IAGOS profiles collected in the same region? Does more frequent denser sampling modify the trends?
- How do SHADOZ total tropospheric column changes (TrCO) compare to OMI/MLS over the 2005-2023 period? Do the satellite data capture the seasonality of sonde-derived trends based on the monthly means used in MLR?

Supplemental material gives a simplified comparison of the 1998-2023 SHADOZ-based trends computed by multiple-linear regression (MLR) compared to the HEGIFTOM analysis for SHADOZ stations evaluated with Quantile-Regression as described in Van Malderen et al. (2024a). Data and analysis methods appear in **Section 2** with Results and Discussion in **Section 3. Section 4** is a summary.

2. Data and Methods of Analysis

2.1 Datasets for ozone

2.1.1 SHADOZ ozonesonde observations

Three data sets are used in our study. For the update to T21, that was based on 1998-2019 SHADOZ v06 ozonesonde data from the website https://tropo.gsfc.nasa.gov/shadoz/Archive.html (https://doi.org/10.57721/SHADOZ-V06), the same records are used with four additional years (2020-2023) of ozone and P-T-U profiles. **Fig. 1** displays locations of the 8 SHADOZ stations that were used in the T21 SHADOZ trends determinations; the new SHADOZ station at Quito (-0.2, -78.4; Cazorla, 2016;

https://doi.org/10.5194/egusphere-2024-3761
Preprint. Discussion started: 30 January 2025

Cazorla et al., 2021; Cazorla and Herrera, 2022) is also shown. **Fig. S1** displays all SHADOZ stations as of September 2024. The ozone profiles are obtained from electrochemical concentration cell ozonesondes coupled to standard radiosondes as described in earlier publications, e.g., Thompson et al., (2003); Thompson et al., (2007); Thompson et al., (2019). The profiles are archived with ozone uncertainties calculated with each individual ozone partial pressure available as separate files at the SHADOZ archive (Witte et al., 2018; WMO/GAW Rep. 268, 2021). Recent evaluations of ozonesonde data have established the quality of the global ECC network. Measurements of total column ozone (TCO) from 60 global stations average within ±2% agreement with total ozone from 4 uv-type satellites since 2005 (Stauffer et al., 2022). About half of the SHADOZ stations exhibit a ~3-5% dropoff in stratospheric ozone (Stauffer et al., 2020) that is not completely understood (Nakano and Morofuji, 2023; Smit et al., 2024). Accordingly, our study only uses ozone data below about 50 hPa, defining the lowermost stratospheric (LMS) ozone as bounded by 15-20 km.

For the updated trends analysis with a multiple linear regression (MLR) model, the same 8 stations used in T21 are analyzed (italicized in **Table 1**, listed in **Table 2**). All have at least 10 years of data between 1998 and 2023, although several have multi-year gaps (**Figs. 2, 3** and **Fig. S2**). These stations (**Table 1**) are located between 5.8N and 14S. For more reliable statistics three of the "stations" or "sites" as they are referred to (**Fig. 1**), are defined by combining profiles from pairs of launch locations abbreviated as follows: SC-Para for San Cristóbal-Paramaribo (dark blue dots in **Fig. 1)**; Nat-Asc for Natal-Ascension (red dots); KL-Java (cyan dots) for Kuala Lumpur-Watukosek (**Table 2**). T21 (see Supplementary Material) describes multiple tests that were conducted to verify that these combinations are statistically justified. Annual cycles in absolute column amounts and anomalies (cf. **Fig. 2**) for the pairs were well-correlated. In T21 total tropospheric columns integrated from sondes ($TrCO_{sonde}$) at the 8 individual stations were also well-correlated (r^2=0.72) with colocated $TrCO_{satellite}$ from OMI/MLS data over the period 2005-2019. It is important to note that the 8 well-correlated sites are within 15 degrees latitude of the equator. The correlation falls to r^2=0.50 when comparisons are made between sondes and satellite columns for the 4 subtropical SHADOZ stations. FT ozone at those locations are seasonally mixtures of tropical and extra-tropical air masses, with latitudes (**Table S1)** spanning Hanoi (+21.0) to Irene (-25.9S).

We have also analyzed trends of tropospheric ozone column and free tropospheric ozone at individual SHADOZ stations using a quantile regression (QR) model, following column definitions and guidelines for the TOAR II/HEGIFTOM (Harmonization and Evaluation of Ground-based Instruments for Free Tropospheric Ozone Measurements) project analysis (Chang et al., 2023). The tropospheric ozone column in HEGIFTOM trends analysis is defined as surface to 300 hPa; the FT is defined as a layer between 300 and 700 hPa and the results are given as ppbv O_3/decade change and %/decade. The QR

https://doi.org/10.5194/egusphere-2024-3761
Preprint. Discussion started: 30 January 2025

trends for 13 SHADOZ sites from 2000 to 2022 are summarized in **Table S1;** a subset of them appear in an evaluation of ground-based global ozone trends in VanMalderen et al. (2024a).

2.1.2 SHADOZ and IAGOS-SHADOZ blended profiles**.** LMS and FT definitions

The MLR trend analyses (results in **Table 2 and 3**) use SHADOZ profile measurements in several ways. First, the trends are computed using monthly-averaged ozone mixing ratios at 100-m intervals from the surface to 20 km, as described in T21. Second, most results are illustrated as ozone column amounts (Dobson Units; 1 DU = 2.69×10^{16} cm^{-2}) for two FT segments, 5-10 km and 10-15 km, and for the LMS (15-20 km). Trends for ozone and pressure-temperature-humidity (P-T-U) data below 5 km are determined for completeness but are not tabulated because station sampling times and local pollution can vary, giving artifact biases among the individual sites (Thompson et al., 2014). We use 15-20 km for the LMS, because this is where several studies identified wave activity associated with convection and ENSO-La Niña oscillations (Lee at al., 2010; Thompson et al., 2011; Randel and Thompson, 2011; T21) and Randel et al. (2007) identified a distinct ozone annual cycle driven by the Brewer-Dobson circulation.

A third way of using SHADOZ profiles in the MLR analysis is in a blend with IAGOS aircraft profile measurements within a lower FT pressure-defined region ("FTp" = 300-700 hPa, cf. Van Malderen et al., 2024a). Calculations in the FTp segment are designed to add more samples within the SHADOZ-labeled combination sites (compare profile numbers in **Tables 2 and 3**) and to augment regional trends in Van Malderen et al. (2024b) where there no results are reported for the equatorial Americas, Atlantic Ocean or African continent. In defining regions for merging SHADOZ and IAGOS observations, we follow locations presented by Tsivlidou et al. (2023). Profiles from the SHADOZ Quito station (2014-2023) and two IAGOS airports (Bogota and Caracas) are added to the SHADOZ SC-Para profiles to define the equatorial Americas for determining trends within the FTp (**Table 3**). Also, for those calculations sonde profiles from the Natal-Ascension pair sites are combined with 13 airports in west Africa (Atlantic+West Africa). Nairobi is combined with IAGOS Addis Ababa profiles. The FTp-designated Equatorial SE Asia consists of KL-Java profiles from SHADOZ combined with IAGOS landing and takeoffs from Kuala Lumpur and Singapore. Time-series for SHADOZ stations and airports for these 4 "regional" sites appear in **Fig. 3** and are defined in **Table 3**. The coordinates of individual SHADOZ stations used in the blended dataset (italicized) with IAGOS airports are given in **Table 1**. Calculations with FTp retain Samoa as a single station.

2.1.3 OMI/MLS satellite and sonde total ozone columns

Trends computed with MLR for total tropospheric ozone columns (TrCO) are based on integrating ozone mixing ratios from the surface to the thermal lapse-rate tropopause. For the equatorial sites in our analyses, the tropopause is typically between 16 and 17 km. Our $TrCO_{sonde}$ columns and trends are compared to $TrCO_{satellite}$, the troposphere ozone columns estimated from the OMI/MLS residual

https://doi.org/10.5194/egusphere-2024-3761
Preprint. Discussion started: 30 January 2025

described by Ziemke et al. (2019; updated in the TOAR II Gaudel et al., 2024). These newest OMI/MLR TrCO estimates have been corrected for a ~1%/decade upward drift in OMI over the past two decades (Gaudel et al., 2024; SI material). The OMI/MLS product is available starting in October 2004. We use monthly average TrCO for both sondes and OMI/MLS between January 2005 and December 2023. These are identical to the data used in SOTC (ref) and in the Gaudel et al. (2024) TOAR II analyses of tropical ozone.

2.2 Methods of trend analysis

2.2.1 Multiple Linear Regression (MLR) model

As in T21 and S24, the Goddard MLR model (original version Stolarski et al., 1991, updated in Ziemke *et al.,* 2019) is used for analysis of monthly mean ozone amounts. The MLR model includes terms for annual and semi-annual cycles and oscillations prevalent in the tropics: QBO, MEI (Multivariate ENSO Index, v2) and IOD DMI (Indian Ocean Dipole Moment Index; only for KL-Java):

$$O_3(t) = A(t) + B(t) + C(t)MEI(t) + D(t)QBO1(t) + E(t)QBO2(t) + F(t)IOD(t) + \varepsilon(t)$$

where t is month. The coefficients are as follows: A through F include a constant and periodic components with 12, 6, 4, and 3 month cycles, where A represents the mean monthly seasonal cycle and B represents the month-dependent linear trend. When annual trends are reported, the B term includes only the 12-month component to generate a single trend value over the period of computation. The model includes data from the MEIv2 (https://www.esrl.noaa.gov/psd/enso/mei/), the two leading QBO EOFs from Singapore monthly mean zonal radiosonde winds at 10, 15, 20, 30, 40, 50, and 70 hPa levels, and IOD DMI (https://psl.noaa.gov/gcos_wgsp/Timeseries/Data/dmi.had.long.data). The ε(t) is the residual, i.e., the difference between the best-fit model and the raw data. T21 noted that the monthly ozone data and MLR model fits for the mid FT (5-10 km) and LMS layers are well-correlated. For the LMS, for example, the correlation coefficients are r = 0.83-0.90 (**Fig. S7** in T21). The IOD DMI term is included for KL-Java because that was the only station where the IOD DMI impact on the ozone trend was reliably detected.

The 95% confidence intervals and p-values for each term in the MLR model as presented here are determined using a moving-block bootstrap technique (10,000 resamples) in order to account for auto-correlation in the ozone time series (Wilks, 1997). The model is applied to ozone anomalies in all cases in order to minimize biases that might arise from intersite ozone differences between pairs for the combined stations: SC-Para, Nat-Asc, KL-Java (**Table 2**). In other words, we calculate ozone anomalies from the individual station's monthly climatology for all profiles before combining the pairs into monthly means and computing the MLR ozone trends. Anomalies are also analyzed for the Nairobi and Samoa station data, although this would be no different than computing MLR trends on the actual ozone timeseries themselves. The MLR model was separately applied to the monthly mean ozone profile anomalies at 100 m resolution, and the monthly mean partial column ozone anomaly amounts from 5-

10 km, 10-15 km, and 15-20 km. The MLR model was also applied to the monthly mean tropopause height (TH) anomaly at each station, defined as the 380 K potential temperature surface (e.g., Wargan et al., 2018). Because TH and LMS ozone trends turn out to be strongly correlated, the MLR analysis was also performed for the ozone column amount anomalies referenced to the tropopause. In that case LMS ozone trends refer to changes in the 5 km above the tropopause with the FT extending from the tropopause to 5km below the tropopause (**Section 3, Table 2**). The MLR model was also applied to total tropospheric column amounts from the sondes ($TrCO_{sonde}$) and corresponding $TrCO_{satellite}$ from OMI/MLS (surface to Tp in **Table 2)**.

Note that recent ozone trends studies and the TOAR II guidelines (Chang et al., 2020; Cooper et al., 2020; Chang et al., 2023) have discouraged the use of nomenclature associated with statistical significance. Therefore, whereas the Figures and Tables presented here refer to trends using terminology of 95% confidence intervals (p-value < 0.05), the most reliable results in **Section 3** (bold in **Tables 2, 3 and S1)** are explicitly stated as based on p-values < 0.05/trends exceeding the 95% confidence interval.

Several studies of tropospheric ozone observations have noted a persistence of COVID-19 perturbations on post-2019 trends after 2019 (Ziemke et al., 2022; Van Malderen et al., 2024a; Van Malderen et al., 2024b). A comparison of the extended SHADOZ mean ozone trends (1998-2023) relative to those from T21 (covering 1998 to 2019), both summarized in **Table 2,** represents the impact of COVID-19 in the deep tropics. Likewise, SHADOZ was initiated at the end of the powerful 1997-1998 ENSO. Accordingly, we applied MLR to the same 5 sites for 2000-2023 to evaluate any artifacts relative to the 1998 to 2023 trends. Those results also appear in **Table 2.**

2.2 Quantile Regression (QR) model

Whereas MLR has been the standard tool for analyzing global total and stratospheric ozone trends, often with satellite data where zonal means can be used, the TOAR II project has recommended using Quantile Regression (QR) as better suited for tropospheric trends. Because it is a percentile-based method (Koenker, 2005), the heterogeneously distributed changes of trends can be estimated, as shown, for example, in Gaudel et al. (2020). To date the TOAR II HEGIFTOM trends studies for observations at individual sites (Van Malderen et al., 2024a) and regionally organized data (Van Malderen et al., 2024b) have been studied with the QR approach. In those studies and for the 13 individual SHADOZ time-series (**Supplemental Table S1**) QR has been applied to the median change of the trends, which is equivalent to the least absolute deviation estimator (i.e. aiming to minimize mean absolute deviation for residuals; Chang et al., 2021). The rationale is that compared to least-squares criterion, a median-based approach is more robust when extreme values or outliers are present. Median trends are estimated based on the following multivariate linear model:

$$\text{Observations}[t] = a0 + a1*\sin(\text{Month}*2\pi/12) + a2*\cos(\text{Month}*2\pi/12)$$

https://doi.org/10.5194/egusphere-2024-3761
Preprint. Discussion started: 30 January 2025

$$+ a3*\sin(Month*2\pi/6) + a4*\cos(Month*2\pi/6) + b*t + c*ENSO[t] + N[t], \qquad \text{Eq. 1}$$

where harmonic functions are used to represent the seasonality, a0 is the intercept, b is the trend value, c is the regression coefficient for ENSO, and N[t] represents the residuals. Autocorrelation is accounted for by using the moving block bootstrap algorithm, and the implementation details are provided in the TOAR statistical guidelines (Chang et al., 2023). In the individual site analyses of HEGIFTOM observations (Van Malderen et al., 2024a), where all individual ozone records (L1) and monthly means (L3) were analyzed, annually averaged trends usually turned out to be the same within uncertainties.

3 Results and Discussion

3.1 Monthly and seasonal ozone climatology at 5 SHADOZ sites

Figure 4 displays the 5-site monthly ozone climatology based on SHADOZ monthly averaged data from the surface to 20 km. Regional differences in vertical structure within the FT are pronounced. For example, the contours representing the 60-90 ppbv range (yellow to red colors) never appear in mid-FT ozone over KL-Java or Samoa (**Figs. 4d,e**). Conversely, FT ozone values $\leq$ 30 ppbv (darkest blue shades) observed over KL-Java and Samoa in the middle FT never appear over the other 3 stations: equatorial Americas (SC-Para, **Fig. 4a**), Nat-Asc or Nairobi (**Figs. 4b,c**). These contrasts may reflect regional differences in ascending vs. descending nodes of the Walker circulation. The latter feature is partly responsible for the tropospheric zonal wave-one (Thompson et al., 2003) that refers to a mean TrCO over the south tropical Atlantic Ocean that is 5% greater than over the western Pacific. There is less regional variability in LMS ozone. At all stations (**Fig. 4**) above ~16 km the colors and contours are nearly uniform over the year. Mixing ratio contours of 100 ppbv and 200 ppbv may appear as a thick white line. The 100 ppbv level is sometimes referred to an ozonopause; typically it is within 1-2 km of the thermal lapse-rate tropopause.

3.2 FT and LMS ozone annual cycle (1998-2023)

The annual cycle of ozone at the two FT layers and for LMS ozone appear as anomalies in **Fig. 5.** FT ozone seasonality (**Figs. 5a,b**) is less uniform than for LMS ozone (**Fig. 5c)** and tropopause height (TH, **Fig. 5d**). We assign TH to the altitude of the 380K potential temperature. Randel et al. (2007) showed that the similar LMS ozone seasonality in the equatorial zone is due to the Brewer-Dobson circulation. The more varied FT ozone cycles in **Figs. 5a,b** are presumably due to a range of different dynamical and chemical influences across the stations. Note that the annual cycle for the pressure- and regionally defined FTp ozone (**Fig. 6** in %**)** resembles that for the corresponding SHADOZ sites in the lower (5-10 km) FT layer in **Fig. 5a**; the magnitudes are similar as well (**Figs. 5** and **6** are illustrated with different scales). In both cases note that there are two seasonal maxima and minima for KL-Java (**Fig. 5a)** and equatorial SE Asia (**Fig. 6a**). The early year minima are associated with intense convective activity (T21, S24) and in August at the onset of the Asian monsoon. However, KL and Watukosek are affected by

https://doi.org/10.5194/egusphere-2024-3761
Preprint. Discussion started: 30 January 2025

seasonal fire activity at the latter end of the rainy seasons. These features were described in detail in Stauffer et al. (2018) using Self-Organizing Map clusters and proxies for convection and fires.

3.3 FT ozone trends: regional and seasonal variability

3.3.1 Trends for 1998-2023

In **Fig.** 7 the trends in %/decade computed with MLR at 100-m intervals, for 1998 to 2023, are displayed (cf. Fig. 6 in T21 for the 1998-2019 trends). Changes in the ozone column amounts for 1998-2023 computed from the model (DU/decade and %/decade) for the two FT layers (5-10 km, 10-15 km) appear in **Fig. 8**. A summary of values for the two layers (and for LMS ozone) is in **Table 2.** The percentage values in **Fig. 7** and **Table 2** are the result of dividing the MLR B(t) term by the A(t) annual cycle of ozone term (Section 2.2.1). The MLR-calculated A(t) annual cycle derived from monthly mean ozone profiles (i.e., no anomaly calculation) is used to convert the B(t) trend in ppmv/decade (profiles) or DU/decade (partial columns) to %/decade. Ozone trends for both percent/decade and DU/decade are given in **Table 2.** Shades of red (blue) in **Fig. 7** represent ozone increases (decreases); cyan hatching denotes trends with p-values < 0.05. The annual mean trends in **Table 2** are computed by taking the average of the 12 monthly trends in DU, and dividing by the mean seasonal ozone in DU to yield the annual percentage trend. The corresponding column trends changes in the FTp layer appear in **Fig. 9** with tabulated trends in **Table 3.** Note that for both **Figs. 8** and **9**, the annual trend for each station at the right of the figure is essentially zero.

For 3 of 5 stations in **Figs. 8a** and **c**, there is a pattern of ozone increase at both FT layers in January to April. Percentage-wise the greatest increases are at KL-Java and Nairobi, ~(10-15)%/decade in March and April. However, SC-Para and Samoa at 5-10 km (**Fig. 8a)** exhibit almost no trend at any time of year; at 5-10 km SC-Para and Nairobi show losses up to 10%/decade in February and (5-10)%/decade losses in August and September. However, **Table 2** displays no trend on an annual basis for SC-Para and Nairobi. Inspection of **Fig. 7** suggests small FT trends at Nat-Asc but **Table 2** displays a +3.4%/decade increase in the 10-15 km layer from 1998-2023. The total column, integrated to the tropopause, TrCO, over Nat-Asc, has increased (1.9± 1.8)%/decade, $p<0.05$. There are no other annually averaged trends in the FT layers but TrCO for KL-Java (KL-Watukosek in **Table 2**), has a similar increase, (2.6± 2.3)%/decade.

Figure 9 monthly ozone trends are based on more than twice the number of profiles as those in the other lower FT layer, **Fig. 8a.** The trends are similar to those in the 5-10 km layer in both magnitude and confidence level (uncertainty). **Table 3** shows no trends ($p<0.05$) at any location. This was unexpected given that Chang et al. (2023) suggest that the uncertainty should decline with more samples and a positive trend might be amplified. For example, adding west African IAGOS data to Natal and Ascension

https://doi.org/10.5194/egusphere-2024-3761
Preprint. Discussion started: 30 January 2025

increased the number of profiles by a factor of > 2.5 (compare **Tables 2** and **3).** Further analysis is needed, including with the QR approach.

3.3.2 FT ozone trends sensitivity to COVID-19 and 1997-1998 ENSO

A comparison of the **Table 2** columns for 1998-2023 relative to those for 1998-2019 (the latter is from T21) reveals little. Only the 10-15 km layer at Nat-Asc has entries with p<0.05 for both periods. The extra 4 years reduced the positive trend slightly. In **Table 2** columns for trends for 2000-2023 can be compared to those for 1998-2023. There is little information in the 2000-2023 column, i.e., no trends anywhere except for the TrCO, total tropospheric column for KL-Java, an area that was well-studied with satellite and some sonde measurements for the period affected by the large ENSO, amplified by the Indian Ocean Dipole pattern (Thompson et al., 2001). After August 1997, as a result of exceptionally high fire activity, ozone increased greatly. That could have meant a smaller change between ozone levels from 1998 through 2023 which would be consistent with a larger, more robust trend for 2000-2023 (4.6%/decade for KL-Java) compared to T21, 2.6%/decade (both p<0.05).

3.4 LMS ozone trends and mean vertical trend over 5 SHADOZ sites

In T21 (Figs. 10 and 11) trends in the LMS (nominally 15-20 km) showed 5-10%/decade decreases for Nat-Asc, KL-Java and SC-Para between July and October. For the same months those locations exhibited a tropopause increase ~100 m/decade. This suggested that the ozone increase was an artifact of a changing tropopause. In other words, if the TH increased more air with relatively lower ozone would be located in the 15-20 km layer. We tested this hypothesis by recomputing ozone column changes referenced to the TH, i.e., evaluated trends in a 5-km thick layer above the TH. The results was that the apparent loss of LMS ozone from July to September or October disappeared. The same analyses were performed with LMS ozone and TH for the 1998-2023 period. The results, shown in **Fig. 10,** are the same as for 1998-2019 (T21).

Whatever the cause(s) of ozone loss in the LMS, it is a feature clearly captured by SHADOZ data as seen in annually averaged ozone trends derived from the analyses displayed in **Fig. 11.** At 18 km the composite trend from the 8 SHADOZ stations analyzed with MLR is (-4±3)%/decade. The mean trend from ~13 to 3 km is zero, albeit with a ±2σ (95%) ±3 %/decade. Only below ~2km is the mean average trend clearly positive. Most of the increase comes from near-surface ozone pollution over equatorial SE Asia (Fig. 6 in S24).

3.5 Total tropospheric ozone trends, TrCO (1998-2023), from OMI/MLR and SHADOZ

Trends for the most recent version of OMI/MLS TrCO were based on monthly mean satellite data and determined with MLR over the period 2005 through 2023. Trends for total tropospheric column ozone

https://doi.org/10.5194/egusphere-2024-3761
Preprint. Discussion started: 30 January 2025

($TrCO_{sonde}$) at the 5 SHADOZ sites for the same period appear in circles on the map in **Fig. 12** where the stippling indicates no trend can be determined. For both OMI/MLS and the sondes (**Fig. 7)** shades of red indicate total column ozone increases; blue represents declining ozone over the period of analysis. The mean annual $TrCO_{sonde}$ trends appear in the two rightmost columns in **Table 2.** In **Fig. 12** OMI/MLS shows trends > 1DU/decade (typically 2-9%/decade) only over equatorial SE Asia and parts of South America and the eastern Pacific at ~5N latitude. Circles indicate locations and trends for the individual SHADOZ stations. The latter display lower trends than OMI/MLS. On a month by month basis the sonde and OMI/MLS trends are compared in **Fig. 13.** In 3 cases the seasonality of TrCO trends from sonde and OMI/MLS are similar and the annually averaged OMI/MLS $TrCO_{satellite}$ trends are not different from zero (symbols at right of each image). However, the seasonality of the KL-Java monthly trends agree well with OMI/MLS; the satellite mean is +5%/decade, gray in **Fig. 13d**. The sonde SC-Para trend (**Fig. 13a**) is quite a bit lower early in the year than the OMI/MLS trends over San Cristóbal and Paramaribo that average +(2-3)%/decade. The Samoa sonde trend and OMI/MLS TrCO trends diverge most of the year; the satellite mean annual trend is close to +10%/decade whereas there is no trend for $TrCO_{sonde}$.

4 Summary

We have updated the 2021 study (Thompson et al., 2021; T21) trends in FT and LMS ozone for 5 stations, Nairobi, Samoa and three combination sites (San Cristóbal-Paramaribo, Natal-Ascension, Kuala Lumpur-Watukosek) for which SHADOZ archiving started in 1998. T21 covered 22 years, ending in 2019 immediately prior to the restrictions imposed by COVID-19. The new analysis has been carried out by adding monthly averaged data from 2000 to 2023 in the Goddard MLR model with standard proxies for the equatorial region. Trends in the FT (5-10km, 10-15 km) and LMS (15-20 km) are illustrated with monthly means and annually averaged trends have been tabulated.

Important new analyses were performed in this study: (1) Trends were determined for the period 2000-2023 to address the question of whether there were impacts of the strong 1997-1998 ENSO-La Niña on long-term SHADOZ trends; (2) The sensitivity of the 1998 to 2023 ozone trends to sample number was explored by doubling the number of profiles analyzed in a modified FT layer using IAGOS aircraft profiles. The additions augmented the SHADOZ data principally over the equatorial Americas, Atlantic (adding in west African airports) and SE Asia. (3) Comparisons of the monthly averaged Aura-derived OMI/MLS satellite product, total tropospheric column ozone to the tropopause ($TrCO_{satellite}$), to monthly mean sonde-derived $TrCO_{sonde}$ were made for 9 equatorial SHADOZ stations; (4) MLR-based based trends for the 8 SHADOZ stations (members of the 5 combined sites), $TrCO_{sonde}$ and the OMI/MLS, $TrCO_{satellite}$, were compared for the 2005-2023 period.

The principal findings are as follows:

https://doi.org/10.5194/egusphere-2024-3761
Preprint. Discussion started: 30 January 2025

- The overall characteristics of T21 trends in the FT and LMS are confirmed with 4 additional years of SHADOZ observations. From 1998 to 2023, regional and seasonal variability remains pronounced with FT ozone increases at 4 of 5 SHADOZ stations in thin layers ~(10-25)%/decade, mostly between January and May. An exception is at SC-Para where there was a 5-10% decrease in between 10-15 km during 1998 to 2023 compared to 1998-2019 (T21). The greatest increases occur in multiple layers below 10 km over Nairobi and KL-Java and between 10-15 km over Samoa. Nonetheless, these features do not translate into annually averaged integrated column trends ($p<0.05$) in the 5-10 km or 10-15 km segments except over Nat-Asc. In summary, adding 4 years of data to equatorial SHADOZ trends, now a trend from 1998-2023, does not modify the T21 picture of little or no FT ozone change.
- Only when the total tropospheric column ($TrCO_{sonde}$) trend is evaluated do Nat-Asc (1.9±1.8)%/decade and KL-Java (2.6±2.3)%/decade) exhibit the slightest trend ($p<0.05$). Examining the 5-station average in vertical form shows a null trend from ~3 to 17 km (± 2% within 2σ up to 7 km and ~± 3% from 7 to 17 km). The marginal overall mean increase, +5%/decade below 3 km, is driven by KL-Java, possibly with a contribution from Nairobi.
- The 1998-2023 trends are not overall different from the pre-COVID T21 trends. With the starting year delayed to 2000, the $TrCO_{sonde}$ KL-Java trend (2000-2023) is almost twice as large as for 1998-2023, indicating an effect of the 1997-1998 ENSO on equatorial SE Asia.
- The T21 LMS ozone and TH trends are confirmed with 4 more years of data. For the layer 15-20 km, ozone losses ~5%/decade from June through October, on average, give an all-site average of -4%/decade at 17.5 km, a value similar to satellite averages (Godin-Beekmann et al., 2022). Re-determining the LMS trends for an ozone column 5 km above the tropopause from 1998 to 2023, causes the trend to disappear, as in T21.
- Doubling the number of profiles in the pressure-defined FT (300-700 hPa) by adding nearby IAGOS aircraft profiles to 4 of the 5 SHADOZ sites does not change the 1998-2023 trends computed with monthly mean MLR. Indeed, no trends are detected with $p<0.05$, i.e., fewer than with the SHADOZ-only profiles. This suggests that current SHADOZ sampling with the 3 combined site records is sufficient.
- When a preliminary calculation of a monthly mean TrCO column capped at 300 hPa for the 8 individual SHADOZ stations (2000-2022) was performed with MLR and QR, the only trends (2-3%/decade at Kuala Lumpur, $p<0.05$) were nearly the same. Using all the data (L1) in QR vs monthly means for Kuala Lumpur increased the trend for that interval to ~6%/decade. Note that the 300 hPa TrCO encompasses ~10km of the 17-km tropospheric ozone column.
- Annually-averaged trends determined with MLR for the OMI/MLS columns, $TrCO_{satellite}$, for 2005 to 2023, for the 8 SHADOZ stations (members of the 5 combined sites) and $TrCO_{sonde}$ overlap

https://doi.org/10.5194/egusphere-2024-3761
Preprint. Discussion started: 30 January 2025

within the uncertainties of each. In both cases the trends are close to zero at SC-Para, Nat-Asc and Nairobi. However, the OMI/MLS $TrCO_{satellite}$ trends are markedly greater than the $TrCO_{sonde}$ at KL-Java and Samoa where the monthly cycles diverge from one another, particularly in the second half of the year. In general, OMI/MLS trends are rarely negative for any month.

How do our updated SHADOZ tropospheric ozone trends compare to those in other studies that use profile data and/or OMI/MLS? The tropical trends study of Gaudel et al. (2024) groups SHADOZ and IAGOS profiles in different ways from this study but for 2005 to 2019, where they compare the in-situ profiles to the updated OMI/MLS, there are similarities. Trends in the equatorial Americas in Gaudel et al., (2024) are generally similar to ours; Gaudel et al. (2024) calculate somewhat higher trends using African airport data separate from Natal and Ascension. As in our study, SE Asian sonde and airport trends appear to give FT column increases ~5%. Near the surface (not discussed here) Gaudel et al. (2024) report very large SE Asia and Indian airport trends.

In T21 we pointed to evidence from changes in apparent wave activity inferred from the 5-site ozonesonde and radiosonde soundings over the period 1998 to 2019 that the early year (February through April) positive trends in FT ozone determined with MLR might be associated with a decrease in equatorial deep convection. S24 focused on linking the strong February-April increase in FT ozone over KL-Java from 1998 to 2022 with corresponding trends in 4 proxies for deep convection, e.g., cloud brightness temperature and OLR changes, Merra-2-based velocity potential at 200 hPa and total column precipitable water. Not only did all the convective signals point to declining convection in the region in February-April, none of the indicators showed trends at any other time of year. A role for changing dynamics needs to be considered in tropical tropospheric ozone increases in recent decades; increasing emissions of ozone precursors are apparently not the only driver. Likewise, apparent losses in LMS ozone appear to be related to tropopause changes during the 1998 to 2023 period.

How do our results compare to FT ozone trends determined for the period 2000 to 2022 in the TOAR II HEGIFTOM activity? Van Malderen et al. (2024a) used both QR and MLR to examine trends in a total tropospheric column (defined from surface to 300 hPa) and FT and lower tropospheric ozone columns. We provided the QR trends, summarized in **Supplemental Table S1**, for 13 SHADOZ stations. Van Malderen et al. (2024a) reported QR and MLR trends for most of the 9 tropical sites listed here and 3 of 4 subtropical sites as well. In VanMalderen et al. (2024b) regional FT trends estimates were reported using grouped SE Asia stations and airports but data from the widely distributed tropical American, African and oceanic SHADOZ station and IAGOS airports were not included. Thus, the updated results for SHADOZ stations documented in this study remain the most reliable reference for ozone trends through the entire tropical troposphere. We provide a definitive standard for evaluating monthly trends

https://doi.org/10.5194/egusphere-2024-3761
Preprint. Discussion started: 30 January 2025

and regional variability of satellite-based products and related models being used for tropical ozone trends assessments and predictions of FT and LMS ozone changes.

Acknowledgments
This study benefitted from discussions with Audrey Gaudel and Kai-Lan Chang (CIRES at NOAA/Chemical Sciences Lab); We thank Kai-Lan Change for the QR code provided for TOAR II. Support is gratefully acknowledged from the NASA Upper Air Research Program (K. W. Jucks, Program Manager), the SAGE III Program (R. Eckman, Manager), and S-NPP and JPSS (J. F. Gleason, Project Scientist). SHADOZ v06 profile data are available at https://tropo.gsfc.nasa.gov/shadoz/Archive.html. OMI/MLS data are available at https://acd-ext.gsfc.nasa.gov/Data_services/cloud_slice/new_data.html.

Competing Interests. All authors declare that we have no competing interests.

References

Cazorla, M., Ozone structure over the equatorial Andes from balloon-borne observations and zonal connection with two tropical seal level sites, *J. Atmos. Chem.,* 2016. https://doi.org/10.1007/s10874-016-9348-2

Cazorla, M., Parra, R., Herrera, E., da Silva, F. R., Characterizing ozone throughout the atmospheric column over the tropical Andes from in situ and remote sensing observations. *Elementa*. 2021 https://doi.org/10.1525/elementa.2021.00019

Cazorla, M., Herrera, E. An ozonesonde evaluation of spaceborne observations in the Andean tropics. *Scientific Reports* **12**, 15942. 2022 https://doi.org/10.1038/s41598-022-20303-7

Chang, K.-L., Cooper, O. R., Gaudel, A., Petropavlovskikh, I., Thouret, V., (2020), Statistical regularization for trend detection: An integrated approach for detecting long-term trends from sparse tropospheric ozone profiles, *Atmos. Chem. Phys.,* 20, 9915-9938, https://doi.org/10.5194/acp-20-9915-2020

Chang, K.-L., Schultz, M.G., Lan, X., McClure-Begley, A., Petropavlovskikh, I., Xu, X., & Ziemke, J.R. (2021). Trend detection of atmospheric time series: Incorporating appropriate uncertainty estimates and handling extreme events. Elem Sci Anth, 9(1), 00035, https://doi.org/10.1525/elementa.2021.00035.

Chang, K. L., Schultz, M. G., Koren, G., & Selke, N. (2023). Guidance note on best statistical practices for TOAR analyses. https://doi.org/10.48550/arXiv.2304.14236.

Cooper, O. R., M. G. Schultz, S. Schröder, K.-L. Chang, A. Gaudel, G. Carbajal Benítez, E. Cuevas, M., Fröhlich, I. E. Galbally, D. Kubistin, X. Lu, A. McClure-Begley, S. Molloy, P. Nédélec, J. O'Brien, S. J. Oltmans, I. Petropavlovskikh, L. Ries, I. Senik, K. Sjöberg, S. Solberg, T. G. Spain, W. Spangl, M. Steinbacher, D. Tarasick, V. Thouret, X. Xu (2020), Multi-decadal surface ozone trends at globally distributed remote locations, Elem Sci Anth, 8(1), p.23. DOI: http://doi.org/10.1525/elementa.420

De Mazière, M., Thompson, A. M., Kurylo, M. J., Wild, J. D., Bernhard, G., Blumenstock, T., Braathen, G. O., Hannigan, J. W., Lambert, J.-C., Leblanc, T., McGee, T. J., Nedoluha, G., Petropavlovskikh, I., Seckmeyer, G., Simon, P. C., Steinbrecht, W., and Strahan, S. E.: The Network for the Detection of Atmospheric Composition Change (NDACC): history, status and perspectives, Atmos. Chem. Phys., 18, 4935–4964, https://doi.org/10.5194/acp-18-4935-2018, 2018.

Gaudel, A., Cooper, O. R., Ancellet, G., Barret, B., Boynard, A., Burrows, J. P., Clerbaux, C., Coheur, P.-F., Cuesta, J., Cuevas, E., Doniki, S., Dufour, G., Ebojie, F., Foret, G., Garcia, O., Granados Muños, M. J., Hannigan, J. W., Hase, F., Huang, G., Hassler, B., Hurtmans, D., Jaffe, D., Jones, N., Kalabokas, P., Kerridge, B., Kulawik, S. S., Latter, B., Leblanc, T., Le Flochmoën, E., Lin, W., Liu, J., Liu, X., Mahieu, E., McClure-Begley, A., Neu, J. L., Osman, M., Palm, M., Petetin, H., Petropavlovskikh, I., Querel, R., Rahpoe, N., Rozanov, A., Schultz, M. G., Schwab, J., Siddans, R., Smale, D., Steinbacher, M., Tanimoto, H., Tarasick, D. W., Thouret, V., Thompson, A. M., Trickl, T., Weatherhead, E., Wespes, C.,Worden, H. M., Vigouroux, C., Xu, X., Zeng, G., and Ziemke, J.: Tropospheric Ozone Assessment Report: Present-day distribution and trends of tropospheric ozone relevant to climate and global atmospheric chemistry model evaluation, Elem. Sci. Anth., 6, 39, https://doi.org/10.1525/elementa.291, 2018.

https://doi.org/10.5194/egusphere-2024-3761
Preprint. Discussion started: 30 January 2025

Gaudel, A., Cooper, O. R., Chang, K-L., Bourgeois, I., Ziemke, J. R., Strode, S. A. Oman, L. D., Sellitto, P., Nedelec, P., Blot, R., Thouret, V., Granier, C., Aircraft observations since the 1990s reveal increases of tropospheric ozone at multiple locations across the Northern Hemisphere, Science Advances, 6, (34), DOI: 10.1126/sciadv.aba8272, 2020

Gaudel, I. Bourgeois, M. Li, K-L. Chang, J. Ziemke, B. Sauvage, R. M. Stauffer, A. M. Thompson, D. E. Kollonige, N. Smith, D. Hubert, A. Keppens, J. Cuesta, K.-P. Heue, P. Veefkind, K. Aikin, J. Peischl, C. R. Thompson, T. B. Ryerson, G. J. Frost, B. C. McDonald, O. R. Cooper, Tropical tropospheric ozone distribution and trends from in situ and satellite data, Atmos. Chem. Phys., Atmos. Chem. Phys., https://doi.org/10.5194/acp-2023-3095, 2024

Godin-Beekmann, S., Azouz, N., Sofieva, V. F., Hubert, D., Petropavlovskikh, I., Effertz, P., Ancellet, G., Degenstein, D. A., Zawada, D., Froidevaux, L., Frith, S., Wild, J., Davis, S., Steinbrecht, W., Leblanc, T., Querel, R., Tourpali, K., Damadeo, R., Maillard Barras, E., Stübi, R., Vigouroux, C., Arosio, C., Nedoluha, G., Boyd, I., Van Malderen, R., Mahieu, E., Smale, D., and Sussmann, R.: Updated trends of the stratospheric ozone vertical distribution in the 60° S–60° N latitude range based on the LOTUS regression model , Atmos. Chem. Phys., 22, 11657–11673, https://doi.org/10.5194/acp-22-11657-2022, 2022.

Koenker, R. (2005). Quantile regression, vol. 38, Cambridge University press, https://doi.org/10.1017/CBO9780511754098

Lee, S., Shelow, D. M., Thompson, A. M., Miller, S. K. (2010). QBO and ENSO variability in temperature and ozone from SHADOZ (1998-2005), *J. Geophys. Res. Atmos.,* 115, D18105, doi: 10.1029/2009JD013320

Muller, K., Tradowsky, J. S., von der Gathen, P., Ritter, C., SharPatris, S., Notholt, J. Rex, M. (2024) Measurement report: The Palau Atmospheric Observatory and its ozonesonde record – continuous monitoring of tropospheric composition and dynamics in the tropical western Pacific, *Atmos. Chem. Phys*., 24, 2169–2193,

https://doi.org/10.5194/acp-24-2169-2024

Nakano, T., and Morofuji, T. (2023) Development of an automated pump-efficiency measuring system for ozonesondes utilizing an airbag-type flowmeter, *Atmos. Meas. Tech.,* 16, 1583–1595, 2023 https://doi.org/10.5194/amt-16-1583-202023.

Randel, W. J., Park, M., Wu, F. (2007). A large annual cycle in ozone above the tropical tropopause linked to the Brewer–Dobson circulation, *J. Atmos. Sci.*, 64, 4479-4488, doi: 10.1175/2007JAS2409.1

Randel, W. J., and Thompson, A. M. (2011), Interannual variability and trends in tropical ozone derived from SHADOZ ozonesondes and SAGE II satellite data, *J. Geophys. Res. Atmos.*, 116, D07303, doi:10.1029/ 2010JD015195

Smit, H. G. J., Poyraz, D., Van Malderen, R., Thompson, A. M., Tarasick, D. W., Stauffer, R. M., Johnson, B. J., Kollonige, D. E., New insights from the Jülich Ozone-Sonde Intercomparison Experiments: Calibration functions traceable to one ozone reference instrument, Atmos. Meas. Tech., 17, 73–112, https://doi.org/10.5194/amt-17-73-2024, 2024

Stauffer, R. M., Thompson, A. M., Witte, J. C. (2018). Characterizing global ozonesonde profile variability from surface to the UT/LS with a clustering technique and MERRA-2 reanalysis, *J. Geophys. Res. Atmos. Atmos*., 123, 6213–6229, https://doi.org/10.1029/2018JD028465

Stauffer, R. M., Thompson, A. M., Kollonige, D. E., Witte, J. C., Tarasick, D. W., Davies, J., et al. (2020). A post-2013 dropoff in total ozone at a third of global ozonesonde stations: Electrochemical concentration cell instrument artifacts? *Geophys. Res. Lett*., 47, e2019GL086791. https://doi.org/10.1029/2019GL086791

Stauffer, R. M., Thompson, A. M., D. E. Kollonige, D. W. Tarasick, R. Van Malderen, H. G. J. Smit, H. Vömel, G. A. Morris, B. J. Johnson, P. D. Cullis, R. Stübi, J. Davies, M. M. Yan, An examination of the recent stability of ozonesonde global network data, *Earth Space. Sci.,* https://doi.org/10.1029/2022EA002459, 2022.

Stauffer, R. M., Thompson, A. M., Kollonige, D. E., Komala, N., Khirzin Al-Ghazali, H., D. Y. Risdianto, A. Dindang, A. F. bin Jamaluddin, M. Kumar Sammathuria, N. Binti Zakaria, B. J. Johnson, P. D. Cullis, Dynamical drivers of free-tropospheric ozone increases over equatorial Southeast Asia, Atmos. Chem. Phys.,

https://doi.org/10.5194/acp-24-5221-2024, 2024

Stolarski, R. S., Bloomfield, P. R., McPeters, R. D., Herman, J. R. (1991). Total ozone trends deduced from Nimbus 7 TOMS data, *Geophys. Res. Lett*., 18, 1015-1018, https://doi.org/10.1029/91GL01302

Thompson, A. M., Witte, J. C., Hudson, R. D., Guo, H., Herman, J. R., Fujiwara, M. (2001) Tropical tropospheric ozone and biomass burning, *Science,* 291, 2128-2132

https://doi.org/10.5194/egusphere-2024-3761
Preprint. Discussion started: 30 January 2025

Thompson, A. M., Witte, J. C., McPeters, R. D., Oltmans, S. J., Schmidlin, F. J., J. A. Logan, J. A., et al. (2003) Southern Hemisphere ADditional Ozonesondes (SHADOZ) 1998-2000 tropical ozone climatology. 1. Comparison with TOMS and ground-based measurements*, J. Geophys. Res. Atmos.,* 108, 8238, doi: 10.1029/2001JD000967

Thompson, A. M., J. C. Witte, H. G. J. Smit, S. J. Oltmans, B. J. Johnson, V. W. J. H. Kirchhoff, F. J. Schmidlin, Southern Hemisphere Additional Ozonesondes (SHADOZ) 1998-2004 tropical ozone climatology. 3. Instrumentation, Station Variability, Evaluation with Simulated Flight Profiles, *J. Geophys. Res.*, 112, D03304, doi: 10.1029/ 2005JD007042, 2007

Thompson, A. M., Allen, A. L., Lee, S. Miller, S. K., Witte, J. C. (2011). Gravity and Rossby wave signatures in the tropical troposphere and lower stratosphere based on Southern Hemisphere Additional Ozonesondes (SHADOZ), 1998–2007, *J. Geophys. Res. Atmos.*, 116, D05302, doi:10.1029/2009JD013429

Thompson, A. M., S. K. Miller, S. Tilmes, D. W. Kollonige, J. C. Witte, S. J. Oltmans, B. J. Johnson, M. Fujiwara, F. J. Schmidlin, G. J. R. Coetzee, N. Komala, M. Maata, M. bt Mohamad, J. Nguyo, C. Mutai, S-Y. Ogino, F. Raimundo Da Silva, N. M. Paes Leme, F. Posny, R. Scheele, H. B. Selkirk,, M. Shiotani, R. Stübi, G. Levrat, B. Calpini, V. Thouret, H. Tsuruta, J. Valverde Canossa, H. Vömel, S. Yonemura, J. Andrés Diaz, N, T. Tan Thanh, H. T. Thuy Ha (2012) Southern Hemisphere Additional Ozonesondes (SHADOZ) ozone climatology (2005-2009): Tropospheric and tropical tropopause layer (TTL) profiles with comparisons to OMI-based ozone products. *J. Geophys. Res*., **117,** D23301, doi: 10.1029/2010JD016911

Thompson, A. M., N. V. Balashov, J. C. Witte, G. J. R. Coetzee, V. Thouret, F. Posny, Tropospheric ozone increases in the southern African region: Bellwether for rapid growth in southern hemisphere pollution? *Atmos. Chem. Phys.,* **14,** 9855-9869, 2014.

Thompson, A. M., Witte, J. C., Sterling, C., Jordan, A., Johnson, B. J., Oltmans, S. J., et al. (2017). First reprocessing of Southern Hemisphere Additional Ozonesondes (SHADOZ) ozone profiles (1998–2016): 2. Comparisons with satellites and ground-based instruments, *J. Geophys. Res. Atmos*., 122, 13,000–13,025, https://doi.org/10.1002/2017JD027406

Thompson, A. M., R. M. Stauffer, K. Wargan, J. C. Witte, D. E. Kollonige, J. R. Ziemke, Regional and seasonal trends in tropical ozone from SHADOZ profiles: Reference for models and satellite products, J. Geophys. Res., https://agupubs.onlinelibrary.wiley.com/doi/10.1029/2021JD034691, 2021.

Thouret, V., Clark, H., Petzold, A., Nédélec, P. & Zahn, A. (2022). IAGOS: Monitoring Atmospheric Composition for Air Quality and Climate by Passenger Aircraft. (pp. 1-14). https://doi.org/10.1007/978-981-15-2527-8_57-1

Tsivlidou, M., Sauvage, B., Bennouna, Y., Blot, R., Boulanger, D., Clark, H., Le Flochmoën, E., Nédélec, P., Thouret, V., Wolff, P. & Barret, B. (2023). Tropical tropospheric ozone and carbon monoxide distributions: characteristics, origins, and control factors, as seen by IAGOS and IASI. (Vol. 23, pp. 14039-14063). https://doi.org/10.5194/acp-23-14039-2023

Van Malderen, R., Thompson, A. M., Kollonige, D. E. et al. Global Ground-based Tropospheric Ozone Measurements: Reference data and trends from individual sites (2000-2022) from the HEGIFTOM homogenized ground-based profile ozone data sets, Atmos. Chem., Phys., submitted, 2024a.

Van Malderen, R., et al. Global Ground-based Tropospheric Ozone Measurements: Regional tropospheric ozone column trends (2000-2022) from the HEGIFTOM homogenized ground-based profile ozone data sets, Atmos. Chem., Phys., submitted, 2024b

Wilks, D.S. (1997). Resampling Hypothesis Tests for Autocorrelated Fields, *J. Climate*, 10 (1), 65-82, https://doi.org/10.1175/1520-0442(1997)010<0065:RHTFAF>2.0.CO;2

Witte, J. C., Thompson, A. M., Smit, H. G. J., Fujiwara, M., Johnson, B. J., et al. (2018). First reprocessing of Southern Hemisphere ADditional Ozonesondes (SHADOZ) profile records (1998-2016): 3. Methodology and evaluation, *J. Geophys. Res. Atmos*., 123, doi:10.1002/2017JD027791

Zhang, Y. Cooper, O. R., Gaudel, A., Thompson, A. M., Nédelec, P., Ogino, S.-Y., West, J. J. (2016). Equatorward redistribution of emissions dominates the 1980 to 2010 tropospheric ozone change, *Nature-Geoscience*, doi: 10.1038/NGEO2827

Ziemke, J. R., and Chandra, S., (2003) Madden-Julian Oscillation in tropospheric ozone, *J. Geophys. Res.,* https://doi.org/10.1029/2003GL018523, 2023.

https://doi.org/10.5194/egusphere-2024-3761
Preprint. Discussion started: 30 January 2025

Ziemke, J. R., Chandra, S., Duncan, B. N., Froidevaux, L., Bhartia, P. K., Levelt, P. F., Waters, J. W. (2006). Tropospheric ozone determined from Aura OMI and MLS: Evaluation of measurements and comparison with the Global Modeling Initiative's Chemical Transport Model, *J. Geophys. Res.,* 111, D19303, https://doi.org/10.1029/2006JD007089.

Ziemke, J. R., L. D. Oman, S. A. Strode, A. R. Douglass, M. A. Olsen, R. D. McPeters, P. K. Bhartia, L. Froidevaux, G. J. Labow, J. C. Witte, A. M. Thompson, D. P. Haffner, N. A. Kramarova, S. M. Frith, L. K. Huang, G. R. Jaross, C. J. Seftor, M. T. Deland, S. L. Taylor Trends in global tropospheric ozone Inferred from a composite record of TOMS/OMI/MLS/OMPS satellite measurements and the MERRA-2 GMI simulation, *Atmos. Chem. Phys.*, 19, 3257–3269, 2019. https://doi.org/10.5194/acp-19-3257-2019

Ziemke, J. R,, Kramarova, N. A., Frith, S. M., Huang, L. K., Haffner, D., Wargan, K.,, Lamsal, L. N., Labow, G. J., Bhartia, P. K., (2022) NASA Satellite Measurements Show Global-Scale Reductions in Free Tropospheric Ozone in 2020 and Again in 2021 During COVID-19, *Geophys. Res., Lett.* https://doi.org/10.1029/2022GL098712

Tables and Figures – Thompson et al., 27 Nov 1630 ET

Table 1. List of the 27 total SHADOZ and IAGOS sites, and their metadata, used in this analysis.

Site	Country	Observation Network	Latitude	Longitude	Altitude (m)
Abidjan (ABJ)	Cote d'Ivoire	IAGOS	5.25	-3.93	6
Accra (ACC)	Ghana	IAGOS	5.61	-0.17	62
Addis Ababa (ADD)	Ethiopia	IAGOS	8.98	38.80	2326
Ascension Island	United Kingdom	SHADOZ	-7.58	-14.24	85
Bogota (BOG)	Colombia	IAGOS	4.70	-74.14	2548
Brazzaville (BZV)	Congo (Brazzaville)	IAGOS	-4.26	15.25	319
Caracas (CCS)	Venezuela	IAGOS	10.60	-67.01	71
Cotonou (COO)	Benin	IAGOS	6.35	2.39	6
Douala (DLA)	Cameroon	IAGOS	4.01	9.72	10
Hanoi	Vietnam	SHADOZ	21.01	105.80	6
Hilo, Hawaii	United States	SHADOZ	19.43	-155.04	11
Irene	South Africa	SHADOZ	-25.90	28.22	1524
Kinshasa (FIH)	Congo (Kinshasa)	IAGOS	-4.39	15.45	313
Koror	Palau	SHADOZ	7.34	134.47	23
Kuala Lumpur	Malaysia	SHADOZ	2.73	101.27	17
Kuala Lumpur (KUL)	Malaysia	IAGOS	2.76	101.71	21
Lagos (LOS)	Nigeria	IAGOS	6.58	3.32	41
Libreville (LBV)	Gabon	IAGOS	0.46	9.41	12
Lome (LFW)	Togo	IAGOS	6.17	1.25	22
Luanda (LAD)	Angola	IAGOS	-8.85	13.23	74
Malabo (SSG)	Equatorial Guinea	IAGOS	3.76	8.72	23
Nairobi	Kenya	SHADOZ	-1.27	36.80	1795
Natal	Brazil	SHADOZ	-5.42	-35.38	42
Pago Pago	American Samoa	SHADOZ	-14.23	-170.56	77
Paramaribo	Suriname	SHADOZ	5.80	-55.21	23
Port Harcourt (PHC)	Nigeria	IAGOS	5.01	6.95	27
Quito	Ecuador	SHADOZ	-0.20	-78.44	2414

https://doi.org/10.5194/egusphere-2024-3761
Preprint. Discussion started: 30 January 2025

Reunion Island	France	SHADOZ	-21.06	55.48	10
San Cristobal	Ecuador	SHADOZ	-0.89	-89.61	8
Sao Paulo (GRU)	Brazil	IAGOS	-23.43	-46.48	750
Singapore (SIN)	Singapore	IAGOS	1.36	103.99	7
Suva	Fiji	SHADOZ	-18.13	178.40	6
Watukosek, Java	Indonesia	SHADOZ	-7.46	112.43	50
Yaounde (NSI)	Cameroon	IAGOS	3.70	11.55	694

https://doi.org/10.5194/egusphere-2024-3761
Preprint. Discussion started: 30 January 2025

Table 2. SHADOZ metadata: number of profiles, annual trends. Each row indicates a different segment: 5-10km, 10-15km, 15-20km, TH-5km to TH, TH to TH +5km, and surface to Tp (tropopause). Periods analyzed (columns) are 1998-2019 (T21), 1998-2023, 2000-2023; 2005-2023 for OMI/MLR comparisons in total tropospheric ozone column amount (TrCO). Annually-averaged MLR partial column ozone linear trends are shown DU per decade and in percent per decade, with the 95% confidence interval. Trends with p-values <0.05 are shown in bold.

SHADOZ T21 Updated MLR FT Ozone Trends										
Station	Altitude Range	Number of Profiles	1998-2019 T21 Annual Trend ± 2*sigma (DU/decade)	1998-2019 T21 Annual Trend ± 2*sigma (%/decade)	1998-2023 Annual Trend ± 2*sigma (DU/decade)	1998-2023 Annual Trend ± 2*sigma (%/decade)	2000-2023 Annual Trend ± 2*sigma (DU/decade)	2000-2023 Annual Trend ± 2*sigma (%/decade)	2005-2023 Annual Trend ± 2*sigma (DU/decade)	2005-2023 Annual Trend ± 2*sigma (%/decade)
San Cristobal – Paramaribo	5-10km	1370	0.2±0.3	1.9±3.1	-0.1±0.3	-0.9±3.7	-0.1±0.3	-1.2±3.8	-0.3±0.5	-3.6±5.1
	10-15km		0.1±0.2	1.5±4.0	-0.2±0.3	-3.5±4.5	-0.2±0.3	-4.0±4.4	**-0.4±0.4**	**-6.6±6.5**
	15-20km		**-0.4±0.4**	**-3.1±2.8**	**-0.5±0.4**	**-3.9±2.9**	-0.4±0.4	-2.8±3.2	-0.4±0.7	-3.3±5.5
	TH-5km to TH		0.0±0.2	0.2±4.2	-0.2±0.3	-2.9±5.1	-0.2±0.3	-2.9±5.2	-0.3±0.4	-5.9±7.5
	TH to TH+5km		0.2±0.6	0.6±2.3	-0.3±0.7	-1.2±2.6	-0.3±0.8	-1.1±2.9	-0.4±1.3	-1.5±4.5
	TrCO, surf-Tp		NA	NA	-0.3±0.9	-1.0±3.3	-0.2±1.0	-0.8±3.6	-0.4±1.6	-1.4±5.9
Natal - Ascension Island	5-10km	1646	0.2±0.3	1.6±2.3	0.2±0.3	1.9±2.2	0.1±0.2	0.5±1.8	0.0±0.4	0.3±2.9
	10-15km		**0.3±0.2**	**3.9±2.8**	**0.2±0.2**	**3.4±2.9**	0.1±0.2	1.7±2.4	0.1±0.3	0.7±3.8
	15-20km		-0.0±0.3	-0.4±2.4	-0.1±0.3	-1.0±2.3	-0.2±0.3	-1.4±2.6	-0.3±0.5	-2.4±3.8
	TH-5km to TH		**0.3±0.2**	**4.7±2.7**	**0.2±0.2**	**3.4±2.9**	0.1±0.2	1.7±2.4	0.0±0.2	0.2±3.3
	TH to TH+5km		0.5±0.5	1.9±1.9	0.2±0.7	0.9±2.7	-0.0±0.6	-0.1±2.5	-0.4±0.9	-1.6±3.7
	TrCO surf-Tp		NA	NA	**0.7±0.6**	**1.9±1.8**	0.3±0.7	0.9±1.9	0.3±1.0	1.0±2.8
Nairobi	5-10km	976	0.1±0.3	1.2±3.1	0.1±0.3	0.5±3.0	0.1±0.4	1.0±3.5	-0.0±0.7	-0.3±6.3
	10-15km		-0.0±0.2	-0.2±3.4	-0.1±0.2	-1.5±3.2	-0.1±0.3	-1.9±4.2	-0.2±0.6	-2.4±8.2
	15-20km		0.1±0.3	0.6±2.5	0.1±0.5	0.9±3.9	0.3±0.5	2.4±4.2	0.7±0.9	5.6±6.9
	TH-5km to TH		0.0±0.2	0.7±3.2	-0.0±0.2	-0.0±2.5	-0.0±0.2	-0.1±3.3	-0.0±0.4	-0.2±6.1
	TH to TH+5km		0.5±0.7	1.9±2.7	0.4±0.9	1.4±3.5	0.5±1.1	1.7±4.2	1.2±1.7	4.5±6.3
	TrCO, Surf-Tp		NA	NA	0.3±0.7	1.1±2.5	0.3±0.9	1.0±3.2	-0.4±1.5	-1.5±5.2
Kuala Lumpur - Watukosek	5-10km	870	0.1±0.2	1.9±3.0	0.1±0.2	1.0±2.5	0.1±0.2	1.0±3.1	-0.1±0.3	-1.2±4.3
	10-15km		-0.0±0.1	-0.6±3.3	0.0±0.1	1.3±3.6	0.1±0.2	2.9±4.2	0.2±0.2	4.3±6.6
	15-20km		**-0.7±0.3**	**-5.8±2.8**	-0.3±0.6	-2.4±4.8	-0.1±0.6	-0.4±5.3	0.6±0.8	5.2±6.8
	TH-5km to TH		-0.1±0.1	-3.2±3.3	0.0±0.2	0.8±5.7	0.1±0.2	2.6±6.8	0.2±0.3	5.1±8.8
	TH to TH+5km		-0.1±0.8	-0.5±3.0	0.2±1.1	0.9±4.2	0.3±1.2	1.1±4.5	**1.7±1.0**	**7.0±4.0**

https://doi.org/10.5194/egusphere-2024-3761
Preprint. Discussion started: 30 January 2025

	TrCO, surf-Tp		NA	NA	**0.6±0.6**	**2.6±2.3**	**1.1±0.7**	**4.6±2.8**	0.7±1.1	3.0±4.6
Samoa	5-10km	928	0.1±0.3	1.4±4.7	0.1±0.3	0.8±4.4	-0.0±0.3	-0.2±4.5	-0.2±0.4	-3.0±5.7
	10-15km		0.1±0.3	2.5±6.5	-0.0±0.4	-1.3±9.2	-0.1±0.4	-3.0±9.4	**-0.4±0.4**	**-10.0±10.0**
	15-20km		-0.4±0.5	-2.8±3.4	-0.3±0.7	-2.3±5.2	-0.4±0.7	-2.9±5.3	**-1.0±0.8**	**-7.0±5.4**
	TH-5km to TH		0.0±0.3	0.2±6.5	-0.1±0.4	-1.7±8.8	-0.1±0.4	-2.5±9.5	**-0.5±0.4**	**-10.6±9.0**
	TH to TH+5km		-0.3±0.7	-0.9±2.4	-0.4±0.9	-1.4±3.1	-0.9±0.9	-2.9±3.0	**-1.2±1.1**	**-3.9±3.7**
	TrCO, surf-Tp		NA	NA	-0.3±1.0	-1.4±4.8	-0.3±1.1	-1.3±5.4	-0.9±1.4	-4.4±6.5

https://doi.org/10.5194/egusphere-2024-3761
Preprint. Discussion started: 30 January 2025

Table 3. SHADOZ and IAGOS combined MLR ozone trends values for FTp (700-300 hPa) partial column for 5 regions: Equatorial Americas, Atlantic and West Africa, East Africa, Equatorial Southeast Asia, and Samoa (individual record). The individual sites are listed for each region. Annually-averaged MLR partial column ozone linear trends are shown DU per decade and in percent per decade, with the 95% confidence interval. Trends with p-values <0.05 are shown in bold.

SHADOZ MLR Regional FT (700-300 hPa) Ozone Trends				
Region Name	**Individual SHADOZ & IAGOS Locations (IAGOS regions in bold)**	**Number of Profiles**	**1998-2023 Annual Trend ± 2*sigma (DU/decade)**	**1998-2023 Annual Trend ± 2*sigma (%/decade)**
Equatorial Americas	San Cristobal (Ecuador), Paramaribo (Suriname), Quito (Ecuador), Caracas (Venezuela), Bogota (Colombia)	2821	0.00 ± 0.31	-0.01 ± 2.57
Atlantic and West Africa	Natal (Brazil), Ascension Island (UK); **Central Africa** [Luanda (Angola), Brazzaville (Congo), Kinshasa (Democratic Republic of Congo)], **Gulf of Guinea** [Lomé (Togo), Yaoundé (Cameroon), Douala (Cameroon), Libreville (Gabon), Accra (Ghana), Abidjan (Ivory Coast), Malabo (Equatorial Guinea), Cotonou (Benin), Port Harcourt (Nigeria)], **Lagos** (Nigeria)	4271	0.12 ± 0.39	0.69 ± 2.28
East Africa	Nairobi (Kenya), Addis Ababa (Ethiopia)	1297	0.12 ± 0.38	0.85 ± 2.69
Equatorial Southeast Asia	Kuala Lumpur (Malaysia), Watukosek (Indonesia); **Gulf of Thailand** [Kuala Lumpur (Malaysia), Singapore (Singapore)]	1305	0.16 ± 0.34	1.57 ± 3.25
Samoa	Pago Pago (Am. Samoa)	928	-0.04 ± 0.38	-0.42 ± 3.85

https://doi.org/10.5194/egusphere-2024-3761
Preprint. Discussion started: 30 January 2025

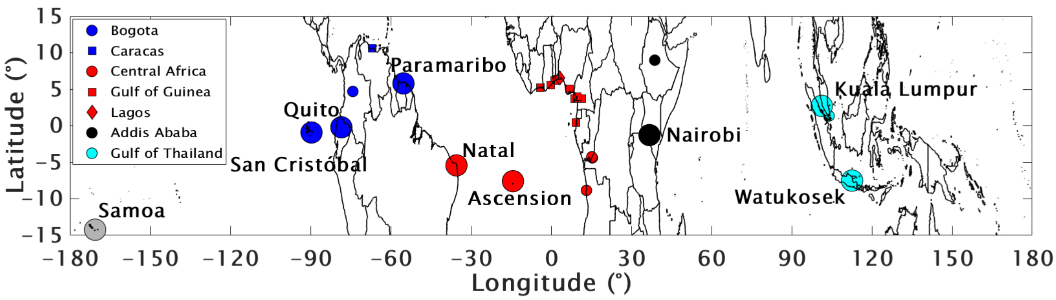

Figure 1. Map of SHADOZ and IAGOS sites used in this study. Stations whose combined records are examined within regions are colored blue for Equatorial Americas, red for Atlantic and West Africa, black for East Africa, cyan for Equatorial Southeast Asia, and gray for Samoa. The 5 SHADOZ sites (2 individual and 3 combined) from T21 are listed in **Tables 1-3**. Individual SHADOZ and IAGOS site names within each region and sample numbers appear in **Table 3.**

https://doi.org/10.5194/egusphere-2024-3761
Preprint. Discussion started: 30 January 2025

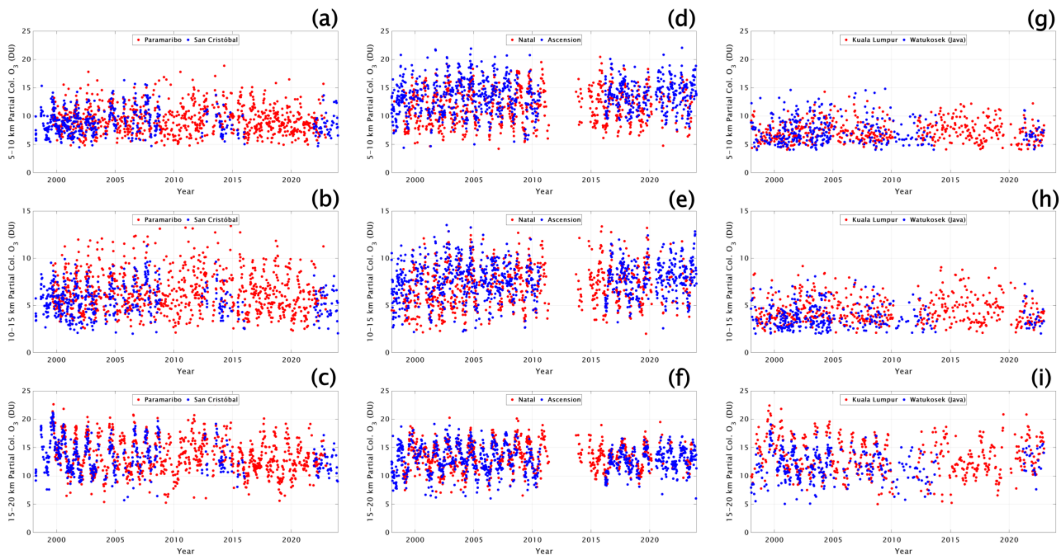

Figure 2. Time-series of ozone column segments (in DU) for the combined SHADOZ stations, for the layers 5-10 km, 10-15 km, 15-20 km for: San Cristóbal-Paramaribo (a-c); Natal-Ascension (d-f); Kuala Lumpur-Watukosek (Java) (g-i). Station coordinates in **Table 1.**

https://doi.org/10.5194/egusphere-2024-3761
Preprint. Discussion started: 30 January 2025

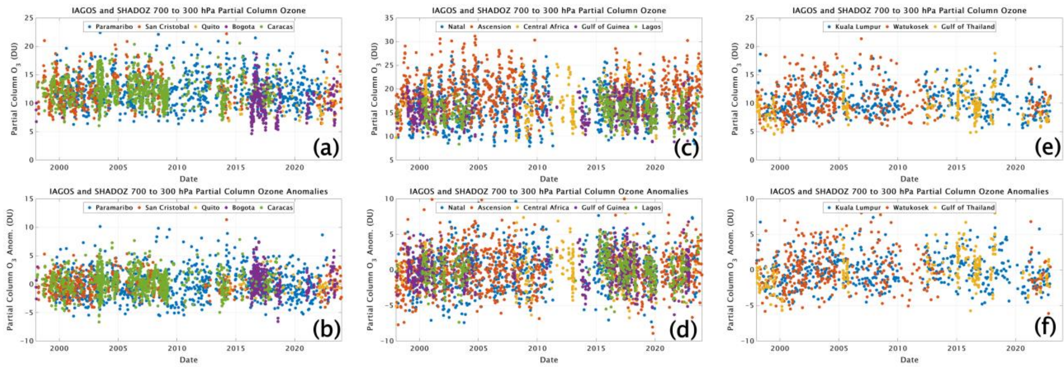

Figure 3. Time-series of SHADOZ and IAGOS partial ozone column amounts and partial ozone column anomalies (in DU) for the pressure-defined mid-free troposphere, FTp (700 to 300 hPa), for (a-b) Equatorial Americas, (c-d) Atlantic and West Africa, and (e-f) Equatorial SE Asia. The listing of the individual sites included in these datasets appears in **Table 3**. Coordinates are in **Table 1.**

https://doi.org/10.5194/egusphere-2024-3761
Preprint. Discussion started: 30 January 2025

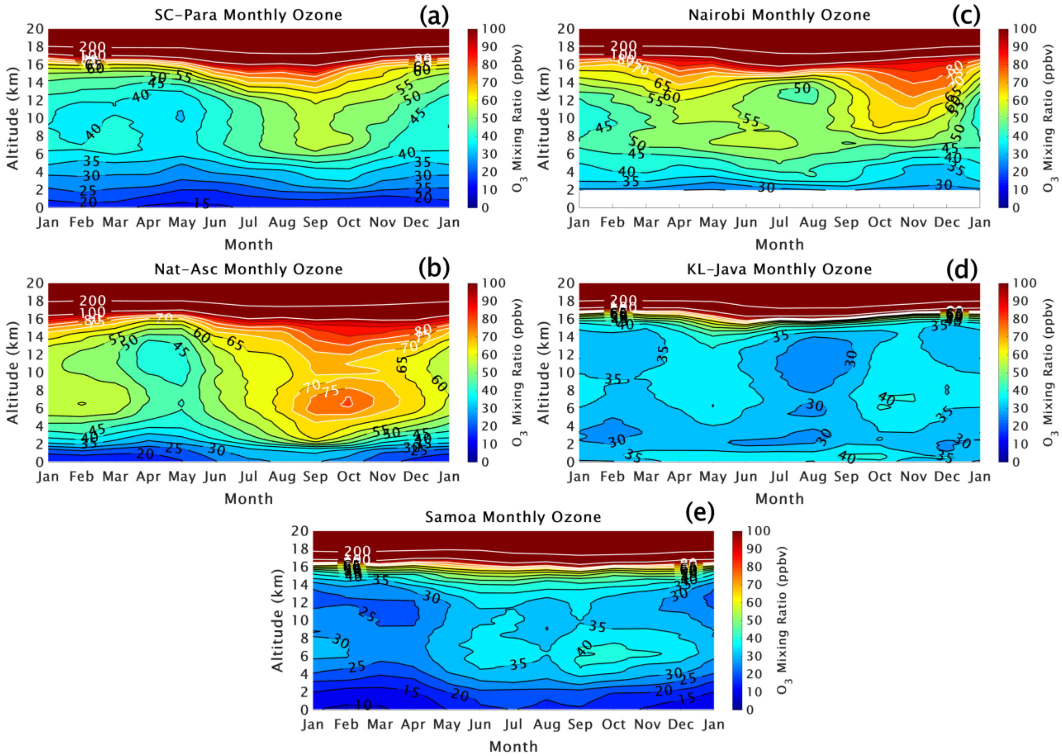

Figure 4. Monthly averaged ozone mixing ratios from the surface to 20 km altitude for the five SHADOZ sites: (a) San Cristóbal – Paramaribo, (b) Natal – Ascension Island, (c) Nairobi, (d) Kuala Lumpur – Watukosek (Java), and (e) Samoa. Colors with black and white contour lines are shown for the ozone mixing ratios in ppbv.

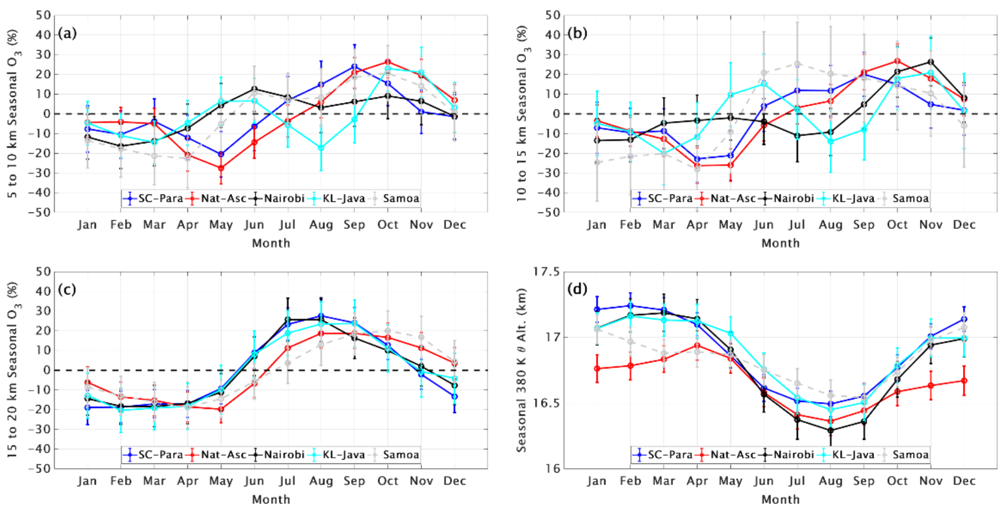

Figure 5. Monthly ozone variability for the five T21 SHADOZ profiles, expressed as percent anomaly from annual mean, determined from the MLR model in the lower and middle FT (5-10 km: a, 10-15 km:

https://doi.org/10.5194/egusphere-2024-3761
Preprint. Discussion started: 30 January 2025

b) and for the LMS (15-20 km: c). The tropopause Height (TH) seasonal cycle (d, in km) is based on the 380 K potential temperature surface from the radiosondes. Dots indicate monthly values; error bars display the 95% confidence intervals.

https://doi.org/10.5194/egusphere-2024-3761
Preprint. Discussion started: 30 January 2025

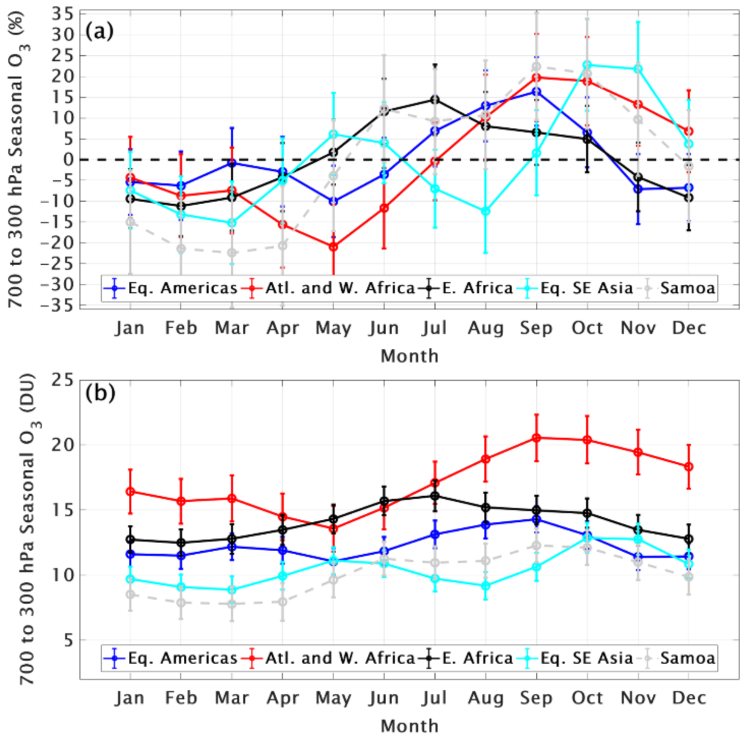

Figure 6. Monthly ozone variability for the five combined SHADOZ+IAGOS regions (defined in **Figure 1** and **Table 3**), expressed as anomaly from annual mean in (a) percent with actual values in DU (b), for FTp (700-300 hPa) column. Dots indicate the monthly values; error bars display the 95% confidence intervals.

https://doi.org/10.5194/egusphere-2024-3761
Preprint. Discussion started: 30 January 2025

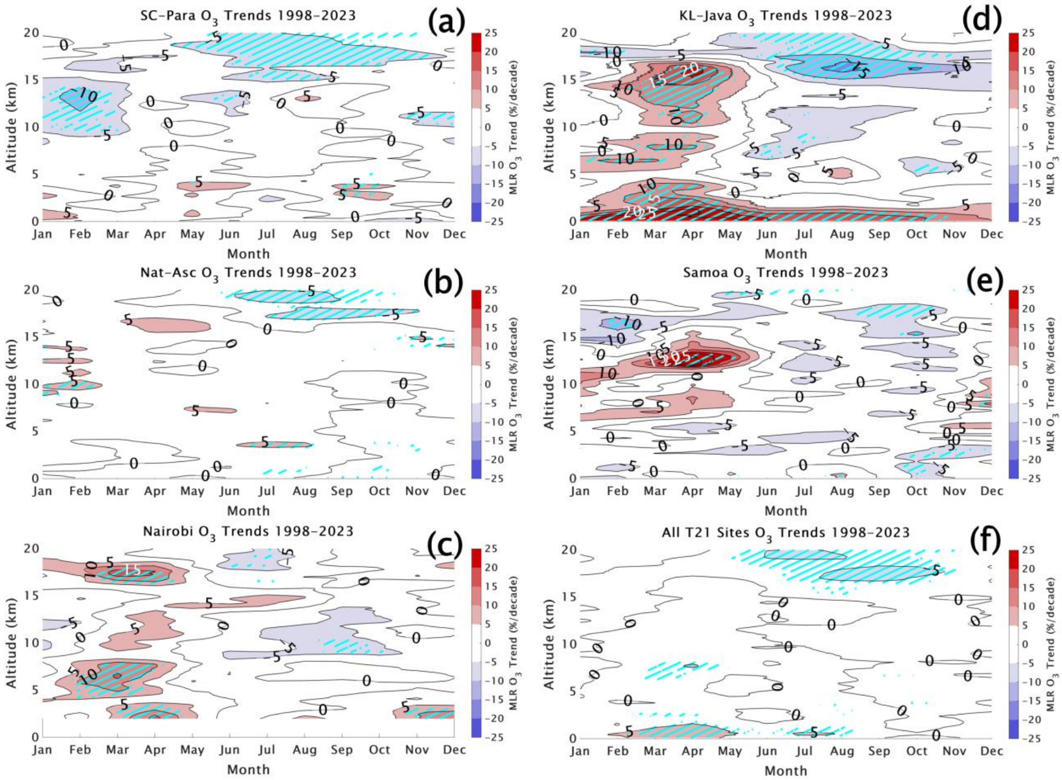

Figure 7. Monthly MLR ozone linear trends from 0 to 20 km in percent per decade for the SHADOZ T21 stations (a) San Cristóbal-Paramaribo (SC-Para); (b) Natal-Ascension (Nat-Asc) (c) Nairobi, (d) Kuala Lumpur-Watukosek (KL-Java); (e) Samoa. This is an update to Figure 6 in T21. In (f), average trends over (a) through (e) are displayed by combining the records from all eight individual T21 SHADOZ stations. Positive trends are shown in red shades and negative trends are shown in blue shades. Trends with p-values <0.05 (exceeding the 95% confidence interval) are shown with cyan hatching.

https://doi.org/10.5194/egusphere-2024-3761
Preprint. Discussion started: 30 January 2025

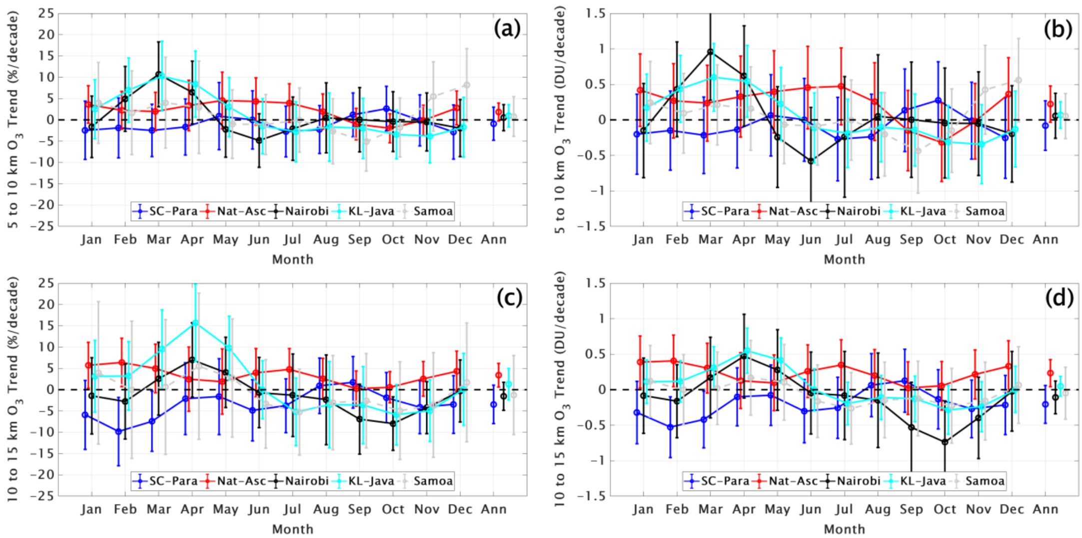

Figure 8. Monthly and annual MLR trends for five T21 SHADOZ sites in lower FT ozone column, integrated from 5-10 km, for (a) %/decade (b) DU/decade; (c) and (d) same as (a) and (b) respectively but for upper FT ozone column (10-15 km), derived from SHADOZ sondes. Dots indicate the monthly and annual trends; error bars display the 95% confidence intervals.

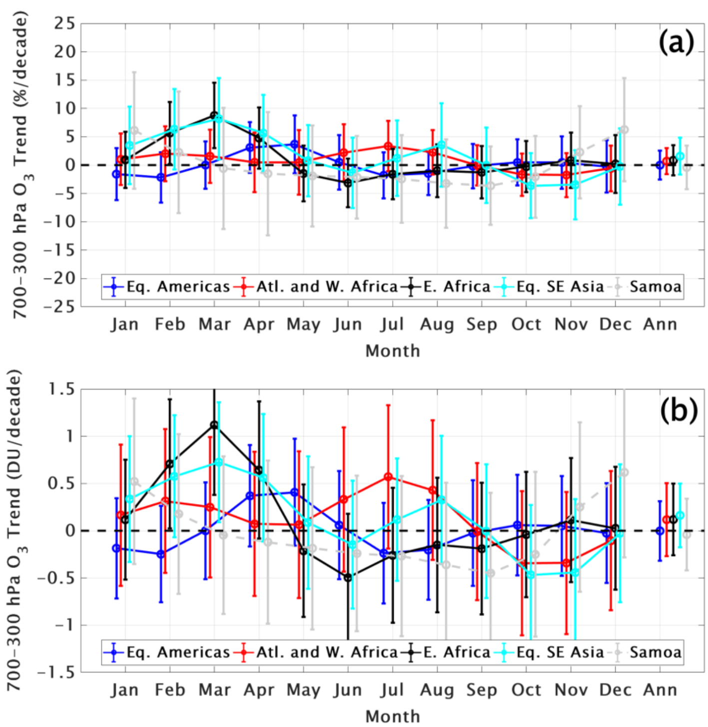

https://doi.org/10.5194/egusphere-2024-3761
Preprint. Discussion started: 30 January 2025

Figure 9. Monthly and annual MLR ozone trends for 5 combined SHADOZ+IAGOS regions, defined in **Table 3**, for FTp column in (a) %/decade and (b) DU/decade. Dots indicate the monthly and annual trends, whereas error bars display the 95% confidence intervals.

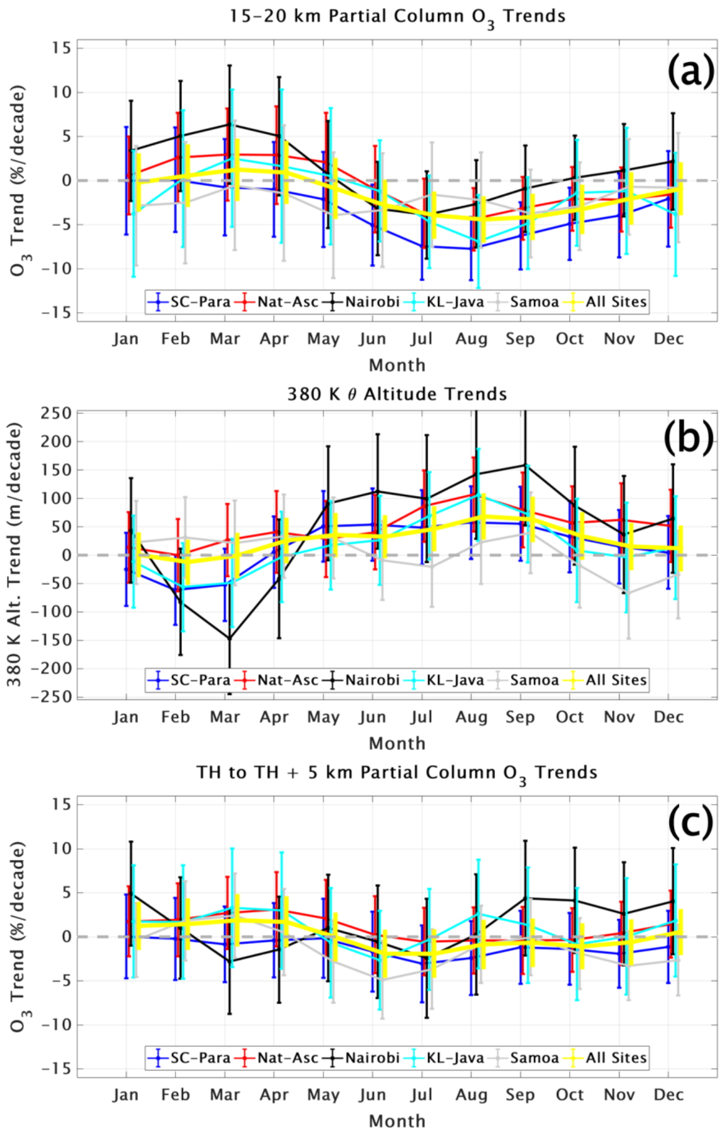

Figure 10. (a) Monthly MLR trends (colored dots) derived from SHADOZ T21 stations highlighting a July-October decrease in LMS ozone in 15-20km layer; yellow dots denote the mean of all T21 stations, with error bars indicating the 95% confidence intervals. (b) Corresponding TH trends (380 K potential temperature; θ) derived from the radiosondes. (c) Same as (a) except trends have been computed for the segments between the tropopause and 5 km above the TH. Compared to (a) the trends in the tropopause referenced ozone column (c) become close to zero throughout the year.

https://doi.org/10.5194/egusphere-2024-3761
Preprint. Discussion started: 30 January 2025

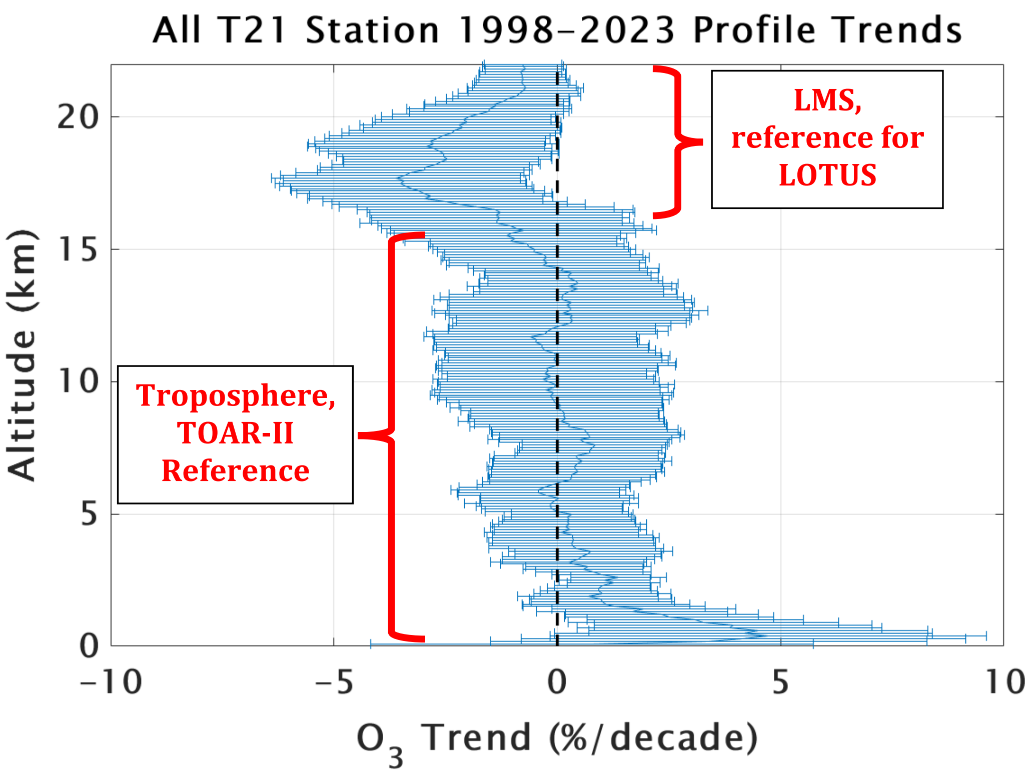

Figure 11. The total mean annual ozone trend (solid blue line), based on mixing ratio changes in 100-m intervals, from the surface to 22 km for all eight T21 SHADOZ profile datasets in %/decade with the 95% confidence interval range denoted. The LMS region of interest to the stratospheric community, e.g., the LOTUS activity, while the tropospheric segment is marked as the primary TOAR-II focus. The -4%/decade trend in LMS ozone is similar to that derived from satellites in that region. The mean change throughout the FT is negligible and within the uncertainty range except below 2 km where mean increases ~+5%/decade are indicated. The near-surface trends are primarily a result of rapid increases in urbanized regions of equatorial SE Asia (Stauffer et al., 2024).

https://doi.org/10.5194/egusphere-2024-3761
Preprint. Discussion started: 30 January 2025

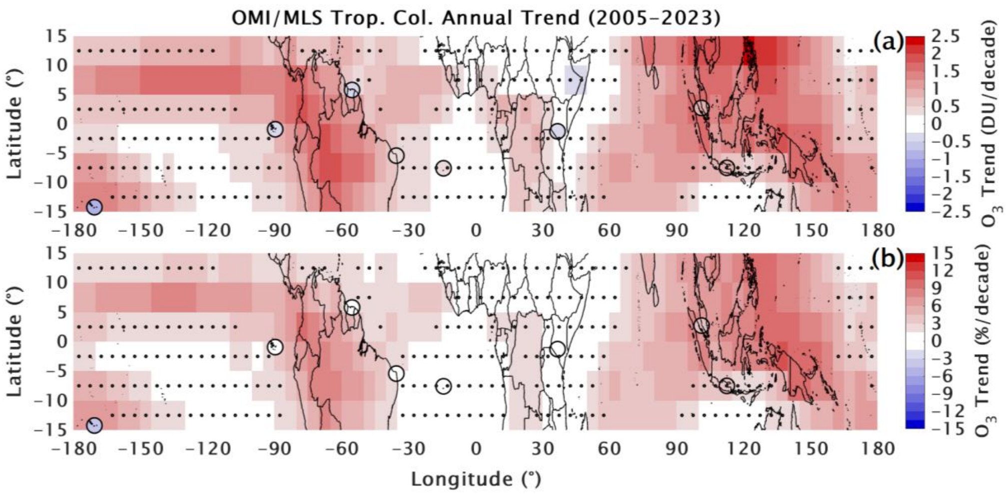

Figure 12. The most recent trends, 2005-2023, shown for the equatorial region based on updated OMI/MLS tropospheric total column ozone ($TrCO_{satellite}$) estimates in which a ~1% per decade positive drift in OMI was corrected. The corresponding SHADOZ-derived $TrCO_{sonde}$ column changes for 2005-2023 are superimposed on the map. Stippling indicates where OMI/MLS trends *do not* exceed the 95% confidence interval (i.e., historically referred to as statistically insignificant).

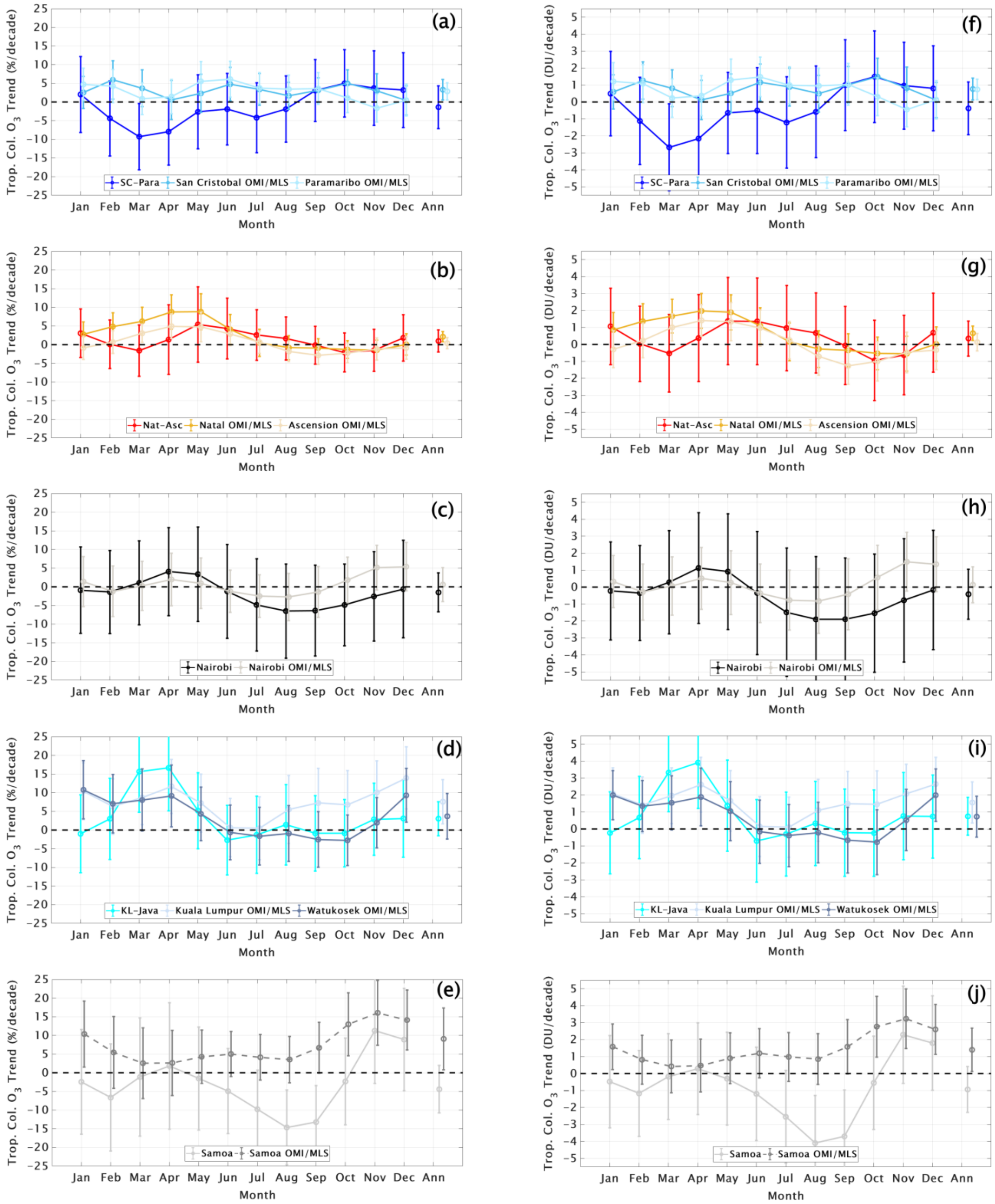

Figure 13. Monthly and annual MLR ozone trends in total tropospheric column (defined using the WMO lapse rate tropopause; TrTO) for the five T21 stations and the OMI/MLS pixel for each individual SHADOZ station each region. Dots indicate the ozone trend in % (a-e) and DU (f-j) per decade; error bars show the 95% confidence intervals.